Geologic Map of the Northern White Hills, Mohave County, Arizona

By Keith A. Howard, Susan S. Priest, Scott C. Lundstrom, and Debra L. Block

Miniature hoodoos formed where a young lag deposit of rounded pebbles and cobbles (2 to 15 cm across), reworked from the Bullhead Alluvium, overlies highly erodible gypsiferous mudstone of the Muddy Creek Formation(?) in northern Detrital Valley, Arizona. Roundstone pebble concentrations reworked downslope can sometimes mimic in-place ancestral Colorado River gravels.

Pamphlet to accompany

Scientific Investigations Map 3372

2017

U.S. Department of the Interior
U.S. Geological Survey

U.S. Department of the Interior
RYAN K. ZINKE, Secretary

U.S. Geological Survey
William H. Werkheiser, Acting Director

U.S. Geological Survey, Reston, Virginia: 2017

Suggested citation:
Howard, K.A., Priest, S.S., Lundstrom, S.C., and Block, D.L., 2017, Geologic map of the northern White Hills, Mohave County, Arizona: U.S. Geological Survey Scientific Investigations Map 3372, pamphlet 31 p., scale 1:50,000, https://doi.org/10.3133/sim3372.

ISSN 2329-132X (online)

Contents

Figures

Tables

Geologic Map of the Northern White Hills, Mohave County, Arizona

By Keith A. Howard, Susan S. Priest, Scott C. Lundstrom, and Debra L. Block

Introduction

The White Hills, part of the Basin and Range Province, lie south of Lake Mead, between the northern Black Mountains to the west and the Grand Wash Cliffs to the east in northwestern Arizona (fig. 1*A*). The map area (fig. 1*B*) consists of three 7.5-minute quadrangles: they are, from west to east, the Senator Mountain NW, the Senator Mountain NE, and the Garnet Mountain NW quadrangles. A north-trending range along the east border of the map area has been called the "Lost Basin Range" by Theodore and others (1987) and later authors. The central part of the map area occupies part of Temple Basin. Ephemeral, intermittent drainages in this high-desert terrain drain northward toward Lake Mead. The National Park Service administers the Lake Mead National Recreation Area in the northern part of the map area, and the Bureau of Land Management administers most of the southern part of the map area (fig. 1*B*). The paved Temple Bar road loops through western and northwestern parts of the map area. Other roads in the map area range from graded to unimproved.

Methods

This map compiles our original work along with mapping and structural data from Lucchitta (1966), Blacet (1975), Laney (1979a,b), Theodore and others (1987), Cascadden (1991), Duebendorfer and Sharp (1998), Blythe (2005), Blythe and others (2010), and Anderson and others (2013). Additional structural data for the Proterozoic rocks can be found in Blacet (1975), Theodore and others (1987), Duebendorfer and Sharp (1998), Duebendorfer and others (2010), and Swaney and others (2010). Additional structural data for the sedimentary rocks near Salt Spring Wash can be found in Duebendorfer and Sharp (1998), Blythe (2005), Blythe and others (2010), and Anderson and others (2013). Petrochemical information can be found in Theodore and others (1987) and Cascadden (1991). Regional mapping by Blacet (1975), Theodore and others (1987), and Cascadden (1991) outlined many basic features of the geologic framework of the area. Geologic maps of adjoining areas by Lucchitta (1966), Blacet (1975), Anderson (1977), Laney (1979a,b), Cascadden (1991), Howard and others (2003), Wallace and others (2005), Blythe (2005), Beard and others (2007, 2011), Faulds and others (2010), Felger and Beard (2010), and Beard and others (2011) provide some regional context. In addition, House and others (2005) and Faulds and others (2008) presented field guides to parts of the map area. Table 1 compiles drill-hole data from the map area. UTM coordinates provided herein refer to 1927 North American datum, as was used on the topographic base map.

Some of our mapping derives from interpretation of MODIS/ASTER Airborne Simulator (MASTER) multispectral images processed by Simon Hook (Jet Propulsion Laboratory) in such a way as to emphasize differences in silicate mineralogy and abundance (Hook and others, 2005; see also, Howard and others, 2003, 2008). Interpretation of geophysical maps (Mariano and Grauch, 1985; Mariano and others, 1986; Langenheim and others, 2010) helped in inferring the presence of concealed faults and in constructing our interpretive cross section. The cross section conjectures many concealed faults in order to portray the style of stratigraphic and structural relations expected in the subsurface. Petrographic descriptions are generalized largely from more detailed descriptions by Theodore and others (1987) and Cascadden (1991).

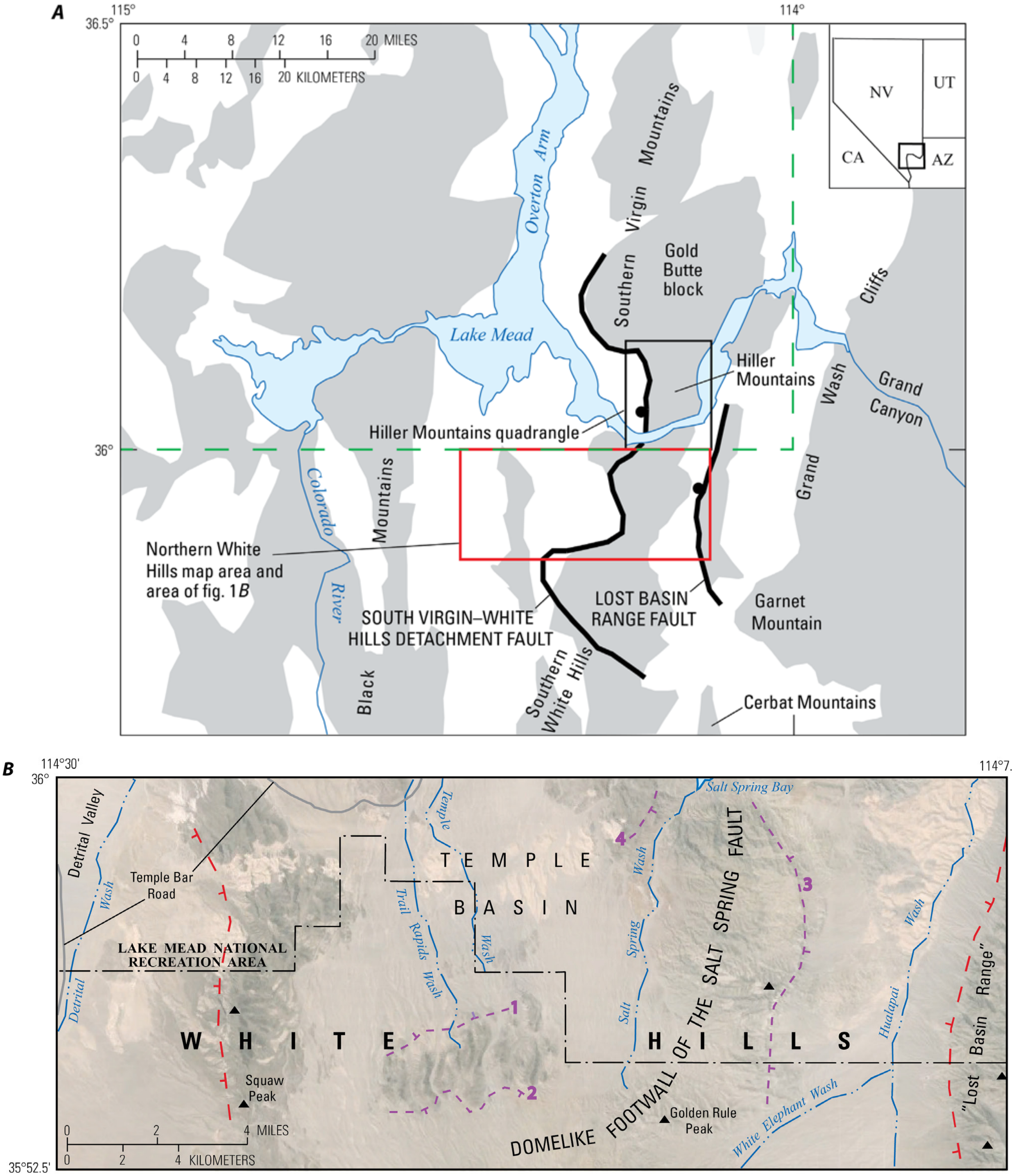

Figure 1. Maps showing northern White Hills map area and geologic and geographic features mentioned in text. *A*, Map showing northern White Hills map area (red outline) relative to highlands (gray shading) and selected faults and geographic features. Thick black lines show two major faults; half-circles on downthrown block. Dashed green line shows outline of Lake Mead 30’×60’ quadrangle. *B*, Satellite image showing geologic and geographic features in northern White Hills map area. Dashed red lines show fault-line scarps; hachures point down scarp (downthrown side). Dashed purple lines show erosional scarps; hachures point down scarp; numbers refer to scarps discussed in text. Image from Google Earth.

Table 1. Drill holes in the northern White Hills map area, Arizona.

[Drill-hole locations not field checked; --, drill holes not plotted on map because precise location was not specified. Abbreviations: *ADWR, Arizona Department of Water Resources database, accessed March 18, 2015, at https://gisweb.azwater.gov/WellRegistry/; n/a, not available; TD, total depth]

Map No.	Well no.; location (reference in parentheses); total depth [notes in brackets]	Modified lithologic or driller's log description; thickness [related map unit (as interpreted herein) in brackets]
1	Hole B-29-21 14add; Detrital Valley (Laney, 1979b); TD=1,392 ft (424 m) [probably included in 11 holes listed in next entry]	Unconsolidated alluvium; 120 ft [Qa2, QTa1] Clay and sandstone; 97 ft [Trbs?] Boulder conglomerate; 185 ft [Trg] Mudstone and siltstone with gypsum and glauberite; 221 ft [Tm, Tmg] Halite and glauberite, clay, silt; 402 ft Coarse, reddish-brown sandstone and siltstone, some halite in upper part, some glauberite beds as thick as 1 ft; 367 ft
--	N/a (11 holes); in or near west side of map area, in T. 29 N., R. 21 W. (Pierce, 1973; Laney, 1979b) [probably includes map no. 1 listed above]. See also, Faulds and others (2016)	Sequence of permeable silt, sand, and gravel [Qa3, Qa2, QTa1, Ta?, Trb], overlying fine-grained beds of the Muddy Creek Formation(?); sequence thickness, 30–437 ft. Eight holes cut halite as much as 715 ft thick. One hole cuts sulfate [Tmg], clastics, halite, and sulfate-clastics, bottoming in conglomerate [Tc]. Evaporite top elevations range from 1,180 to 1,500 ft. Salt top elevations range from 1,109 to 1,357 ft
--	N/a (3 holes); in, or closely adjacent to, northwest corner of map area, in secs. 12, 13, 14, T. 30 N., R. 21 W. (Pierce, 1973)	Encountered calcium sulfate–clastic section [Tmg] that overlies plutonic igneous rock [Tbx?]; clastic section, about 700 ft thick. Evaporite top elevations range from 1,300 to 1,600 ft
2	Well 55-523792; 0.8 km southeast of Golden Rule Peak (location inferred, on basis of driller's report; *ADWR); TD=540 ft (165 m)	Gravel, red conglomerate, and rocks; 315 ft [Qa2?, mostly Xg?] Hard rock, conglomerate, and granite; 225 ft [Xg]
--	N/a; Hualapai Wash (drilled for Rhodes Homes/Sedora Holdings LLC; National Park Service, written commun., 2005); n/a [may refer to some wells that follow]	Drilling to 650–700 ft reportedly encountered cavernous limestone formation [Th] and did not encounter bedrock
3	Well 55-208804; Hualapai Wash, at White Elephant Wash (*ADWR); TD=1,010 ft (308 m)	Gravel; 350 ft [Qa3, Tca, Th] Sand; 60 ft [Th?] Limestone and siltstone; 310 ft [Th] Angular gneiss fragments; 290 ft [Tc, Xg?]
4	Well 55-904437; 1.7 km west of Hualapai Wash, near road to Temple Bar (*ADWR); TD=1,000 ft (305 m)	Gravel; 40 ft [Qa3, Qa2] Claystone; 10 ft [Tdh?] Carbonate, trace of sand and gravel; 150 ft [Th] Clayey, sandy gravel; 80 ft [Th?] Clay; 40 ft [Th?] Clayey, sandy gravel; 240 ft [Th?] Sandy, gravely clay; 40 ft [Th?] Sandy gravel, well lithified; 260 ft [Tc?] Gravelly sand, well lithified; 80 ft [Tc?] Bedrock schist; 60 ft [Xg]

Table 1. Drill holes in the northern White Hills map area, Arizona.—Continued

Map No.	Well no.; location (reference in parentheses); total depth [notes in brackets]	Modified lithologic or driller's log description; thickness [related map unit (as interpreted herein) in brackets]
5	Well 55-904659; Hualapai Wash (*ADWR); TD=400 ft (122 m)	Gravel; 30 ft [Qa4, Qa3] Silty, clayey sand; 20 ft [Tdh] Silty clay; 50 ft [Tdh] Clay, silt, and sand, moderately well lithified; 130 ft [Th] Clay, silt, and sand, well lithified; 30 ft [Th] Silty clay and sand, slightly to moderately well lithified; 60 ft [Th] Silty, sandy clay, with some gravel and metamorphic-rock fragments; 60 ft [Tc] Gneiss, hard; 30 ft [Xg]
6	Well 55-904439; 2 km west of Hualapai Wash, near road to Greggs Hideout (*ADWR); TD=60 ft (18 m)	Sandy gravel; 40 ft [Th?] Bedrock gneiss; 20 ft [Xg]
7	Well 55-904436; 1 km north of Gold Hill Mine (*ADWR); TD= 360 ft (110 m)	Gravel 20 ft [Qa3, Qa2] Loose, sandy gravel and clay; 50 ft [Tm] Cemented sand, gravel, and clay; 150 ft [Tc] Well-lithified, gravelly sand ("black volcanics"); 140 ft [Xg]
8	Well 55-212231; Hualapai Wash (*ADWR); TD=1,199 ft (365 m)	Gravel with sand; 530 ft [Qa3, Tca, Tdh, Th?] Clay; 20 ft [Th?] Sand and clay; 110 ft [Th?] Limestone; 420 ft [Th] Limestone, sand, and clay; 119 ft [Th, Tc?]

Geologic Summary

Neogene Structural and Stratigraphic Framework

The northern White Hills map area lies within the Kingman Uplift, a regional structural high in which Tertiary rocks lie directly on Proterozoic rocks as a result of Cretaceous orogenic uplift and erosional stripping of Paleozoic and Mesozoic strata (Lucchitta, 1966; Bohannon, 1981, 1984). The Miocene Salt Spring Fault forms the major structural boundary in the map area. This low-angle normal fault separates a footwall (lower plate) of Proterozoic gneisses on the east and south from a hanging wall (upper plate) of faulted middle Miocene volcanic and sedimentary rocks and their Proterozoic substrate (Cascadden, 1991; Duebendorfer and Sharp, 1998; Anderson and others, 2001; Faulds and others, 2008; Duebendorfer and others, 2010). The fault is part of the South Virgin–White Hills Detachment Fault (fig. 1*A*), which records significant tectonic extension that decreases from north to south (Fitzgerald and others, 2009; Duebendorfer and others, 2010). Along most of its trace, the Salt Spring Fault dips gently westward, but it also has north-dipping segments along salients (Duebendorfer and others, 2010). A dissected, domelike landscape on the eroded footwall, which contains antiformal salients and synformal reentrants, extends through the map area from Salt Spring Bay southward to the Golden Rule Peak area (fig. 1*B*). The "Lost Basin Range" represents an upthrown block of the footwall, raised on the steeper Lost Basin Range Fault (fig. 1*A*) (Duebendorfer and Sharp, 1998; Swaney and others, 2010).

The Salt Spring Fault, as well as the normal faults that segment its hanging wall, deform rocks that are about 16 to 10 Ma, and younger deposits overlie the faults. Rhyodacitic welded tuff about 15 Ma underlies a succession of geochemically intermediate to progressively more mafic lavas (including alkali basalt) that range from about 14.7 to 8 Ma, interfingered with sedimentary rocks and breccias in the western part of the map area (Cascadden, 1991). Upper Miocene strata record further filling of the extension-formed continental basins. Suggested correlations for the Miocene sedimentary rocks are shown in figure 2. Basins that are still present in the modern landscape reflect the youngest stages of extensional-basin formation, expressed as the downfaulted Detrital Valley and Hualapai Wash basins in the western and eastern parts of the map area, respectively, as well as the north-centrally located, northward-sagged Temple Basin. Pliocene fluvial and piedmont alluvial fan deposits record postextensional basin incision, refilling, and reincision driven by the inception and evolution of the westward-flowing Colorado River, centered north of the map area.

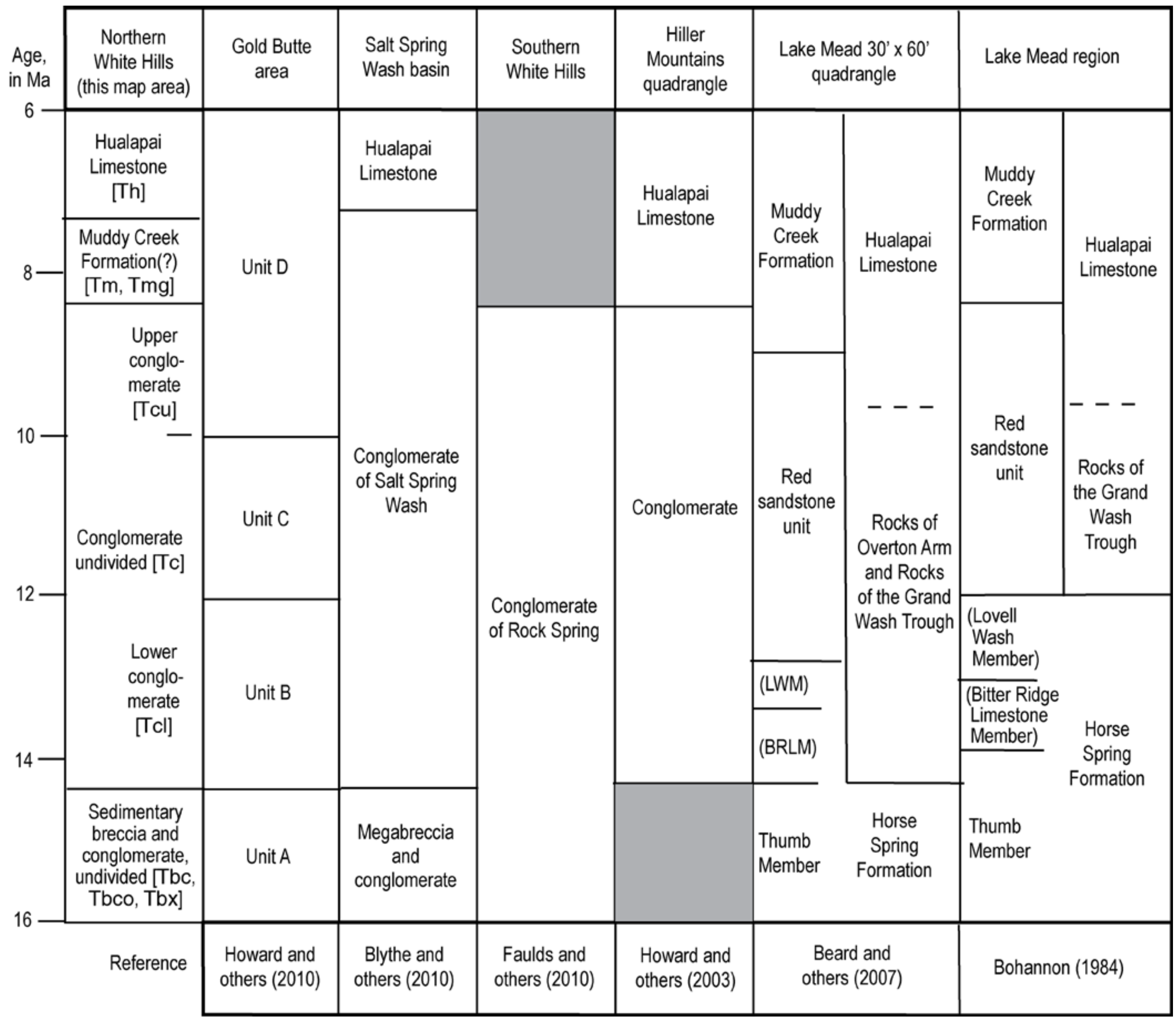

Figure 2. Chart showing suggested generalized correlation of middle and upper Miocene strata in and around White Hills region (see fig. 1*A*). Salt Spring Wash basin occupies north-central parts of northern White Hills map area. Many units are time-transgressive, and some time-transgressive boundaries are shown as dashed lines (see, for example, Beard and others, 2007). Note that northern White Hills map area lacks facies that resemble two upper members (Lovell Wash [LVM] and Bitter Ridge Limestone [BRLM] Members) of the Horse Spring Formation, which are found northwest of Lake Mead (fig. 1*A*). Gray boxes indicate that strata are absent. Map units in northern White Hills map area are shown in brackets.

Proterozoic Basement Rocks

The northern White Hills map area lies in the Arizona Mojave subprovince of Proterozoic crust (Wooden and Dewitt, 1991; Duebendorfer, 2015). Paleoproterozoic gneisses derived from sedimentary and igneous protoliths crop out (in places) in the hanging wall and (widely) in the footwall of the Salt Spring Fault and in the “Lost Basin Range.” Theodore and others (1987) found that quartzofeldspathic gneisses derived from graywacke or arkosic compositions dominate, along with pelitic gneiss and small amounts of metachert, quartzite, metamorphosed-iron formation, and calc-silicate rocks. Theodore and others (1987) described amphibolite-facies prograde metamorphic-mineral assemblages. Supracrustal gneisses in the Cerbat Mountains, about 30 km south of the map area (fig. 1*A*), were deformed between 1,740 and 1,721 Ma and again between 1,719 and 1,682 Ma (Duebendorfer and others, 2001). Orthogneisses that vary in composition from mafic to leucogranitic intrude and, in places, form migmatites within the supracrustal gneisses. Some mafic gneiss, including quartz-poor gneiss, is mapped separately (Xgm) using remote sensing, and it aids in the recognition of geologic structure.

We lithologically correlate the granite of Burro Spring (Yb), which forms a pluton in the northeastern part of the map area, to the Gold Butte Granite (Longwell, 1936) of Mesoproterozoic age in Nevada’s southern Virgin Mountains. Diabase dikes (Yd) of Mesoproterozoic age are mapped in a small exposure in the south-central part of the map area where they intrude gneiss in the hanging wall of the Salt Spring Fault.

Retrograde-metamorphic mineral assemblages overprint many of the higher grade mineral assemblages. Mapped paragneiss is divided into three subunits on the basis of whether garnets are completely (Xgr), partly (Xgp), or not at all (Xgg) replaced by retrograde minerals, following the mapping scheme of Fryxell and others (1992). Areas mapped as these three subunits are small because much of the paragneiss in this map area lacks garnet, in contrast to the areas where the retrograded-garnet mapping scheme had been previously used, 0 to 30 km north of the map area in the southern Virgin and Hiller Mountains (fig. 1*A*) (Fryxell and others, 1992; Howard and others, 2003, 2010; Beard and others, 2007). Paragneiss in the hanging wall of the Salt Spring Fault (in the south-central part of the map area), representing shallow depths in the preextensional crustal column, has garnets that are either fresh or partly retrograded to lower grade mineral assemblages. Some footwall rocks exhumed from below the Salt Spring Fault, on the other hand, contain fully retrograded garnet paragneiss. The degree of garnet retrogression, therefore, increases downward if crustal sections are retrodeformed for Miocene faulting and tilting.

Retrogression of garnets to chloritic psuedomorphs in parts of the Gold Butte block, 10 to 30 km north of the map area (fig. 1*A*), was suggested to relate to Miocene extension and, perhaps, also to Mesozoic events (Fryxell and others, 1992). Muscovite in footwall gneisses in the northern White Hills map area yielded disturbed $^{40}Ar/^{39}Ar$ spectra with apparent ages of about 550 to 379 Ma near Salt Spring Wash and about 900 Ma near Salt Spring Bay, comparable with earlier potassium-argon (K-Ar) results by Theodore and others (1987). The rocks, therefore, have remained at temperatures less than the closure temperature for argon in muscovite (about 350 °C) since well before Cenozoic time (Duebendorfer and Sharp, 1998; Verdel and others, 2011); any higher temperature retrogressive metamorphism is older. We infer that garnet retrogression predates the Miocene extension.

A greenschist-facies chloritic overprint on footwall gneisses near the Salt Spring Fault has been attributed to the Miocene detachment faulting (Duebendorfer and Sharp, 1998; Duebendorfer and others, 2010). Fryxell and others (1992) interpreted similar retrogressive metamorphism (as well as a gently dipping mylonitic foliation) in the Gold Butte block, 10–30 km north of the White Hills map area, as caused by Miocene faulting on the South Virgin–White Hills Detachment Fault.

Synextensional Miocene Rocks

Tilted and faulted sedimentary and volcanic rocks (units Twt, Tbc, and subunits of Tbc [Tbx, Tbco]) nonconformably overlie hanging-wall basement gneisses. The character of the megabreccia (Tbx) and the old conglomerate (Tbco) among these strata implies derivation from Proterozoic rocks exposed by active extensional faults (Duebendorfer and Sharp, 1998). The mapped degree of garnet retrogression in clasts of basement gneiss offers guides to possible provenance in mapped basement gneisses (Howard and others, 2010). For example, gneiss clasts in the Miocene megabreccia in the southwestern part of the map area contain fresh garnet, similar to the garnet-fresh paragneiss (Xgg) exposed in the hanging wall but unlike the retrograded-garnet paragneisses (Xgp, Xgr) mapped in the footwall rocks below the Salt Spring Fault.

Near Salt Spring Wash, two lithologically distinct welded tuff (unit Twt) layers are interlayered with the conglomerate and megabreccia; the more eastern, apparently higher tuff was dated ($^{40}Ar/^{39}Ar$, sanidine) as 15.2 Ma by Duebendorfer and Sharp (1998). Elsewhere in the map area, a single welded tuff (also unit Twt) is recognized in the section, but Cascadden (1991) reported two cooling units in western Temple Basin. The welded tuff(s) are inferred to correlate to the tuff of Mount Davis and (or) the tuff of Bridge Spring, ignimbrites that are found as many as several tens of kilometers to the south and west of the map area (Anderson, 1971; Faulds and others, 1995, 2002, 2010).

A thick basaltic andesite (Tda) sequence herein assigned to the Mount Davis Volcanics overlies and interfingers with the sedimentary breccia and conglomerate (Tbc). Duebendorfer and Sharp (1998) interpreted the basal contact of these mafic volcanic rocks near Salt Spring Wash as a local angular unconformity, indicating that fault-related tilting of the underlying sedimentary breccia and conglomerate (Tbc), and welded tuff (Twt, dated as 15.2 Ma) units was mostly finished when the basaltic andesite (dated as 14.6 Ma) was erupted. More recent mapping of that area (Blythe and others, 2010; Anderson and others, 2013) indicates a more complex, less angular but partly faulted transition from sedimentary strata to the overlying Mount Davis Volcanics. Interfingering relations between basaltic andesite and megabreccia in the southwestern part of the map area are consistent with continued faulting, landsliding, and tilting after eruption of the Mount Davis Volcanics began. The Mount Davis Volcanics in that area transition upward from pyroxene-phyric (Tda) to olivine-pyroxene rocks (in part, mapped separately as Tdo). Local erosional events and progressive tilting during the accumulation of the Mount Davis Volcanics are recorded by interfingered volcanic-clast conglomerate (unit Tdc) (fig. 3) and by angular and erosional unconformities. Upward-fanning stratal dips indicate progressive extensional tilting during deposition from 15.2 to 10.8 Ma (Blythe and others, 2010).

Younger Miocene Rocks

A stratigraphically higher, less tilted series of middle and upper Miocene basalts and sedimentary rocks begins with olivine basalt (unit Tob). This 13- to 12-Ma unit caps a series of faulted mesas in the south-central part of the map area. Younger Miocene units become successively less deformed upward. They consist of the young olivine basalt (Tby), three conglomerate units (Tcl, Tcu, Tc), the Muddy Creek Formation(?) (Tmg, Tm), and the Hualapai Limestone (Th). These units lap southward toward the faulted mesas of the olivine basalt (Tob) and dip gently northward. The (ash-fall) tephra beds (unit Tct) that are within or interbedded with the lower conglomerate (unit Tcl) were dated and correlated as 14.5 to 12.1 Ma in the map area and 10.8 Ma 1 km farther north (Blythe and others, 2010; Howard and others, 2010), which indicates that the lower conglomerate's age spans that of the olivine basalt (Tob).

The Muddy Creek Formation(?) lies in buttress unconformity against the Mount Davis Volcanics. The Muddy Creek Formation(?) largely consists of mudstone (Tm) but, in Detrital Valley, also includes a gypsum facies (Tmg), which reaches nearly 200 m thickness in a drill hole near the northwest corner of the map area (Laney, 1979b). Drilling revealed that the section in Detrital Valley

Figure 3. East-dipping rocks of the Mount Davis Volcanics (Miocene), which consist of dark mafic flows (units Tda, Tdo) and (in middle ground) interbedded reddish-brown volcanic-clast conglomerate (unit Tdc). View is to north into southwestern part of map area. Squaw Peak is on left horizon; downslope, to right of that peak, light-toned, calcrete-covered (unit QTk) ridgelines record remnant Pliocene surfaces.

also includes substantial subsurface halite that covers an area of at least 13 km^2 (table 1; see also, U.S. Geological Survey, 1972; Pierce, 1973; Anderson and Laney, 1975; Laney, 1979b; Faulds and others, 2016). Drilling 3 km north of the southwest corner of the map area revealed clayey halite 123 m thick, beginning at 190 m depth, in addition to more halite in an underlying section of sand and silt (table 1, map no. 1). The gypsum and halite record evaporative conditions during lake and playa deposition.

Deposition of the Hualapai Limestone (Th) culminated the progressive filling of interior basins that had resulted from middle Miocene extension. North of the map area, the limestone interfingers with underlying mudstone of the Muddy Creek Formation(?), and a tephra bed in the limestone correlates to one in the gypsum of the Muddy Creek Formation(?) to the west (also north of the map area), indicating coeval facies transitions (Howard and others, 2003, 2010). Within the map area, the Hualapai Limestone in Temple Basin thickens and overlaps basinward from substrates of the Mount Davis Volcanics onto the young olivine basalt (Tby), two conglomerate units (Tcl, Tcu), and the Muddy Creek Formation(?). In the Hualapai Wash area, the Hualapai Limestone (fig. 4) thins westward on Proterozoic footwall rocks, lapping westward toward the base of an east-facing erosional scarp in the footwall rocks (fig. 1*B*, scarp 3). Detrital-zircon age populations indicate derivation of the Muddy Creek Formation(?) and the Hualapai Limestone from nearby sources (Crossey and others, 2015).


A


B

Figure 4. Structures in the Hualapai Limestone in eastern part of map area. *A*, Soft-sediment boudinage of 1-m-thick white bed in limestone. *B*, Underside (in shadow) of limestone bed showing casts of dimple-shaped depressions between broader hillocks (1.3 m wide and 0.2 m high); these structures, of unknown origin, indent substrate limestone that is capped by clay bed less than 1 cm thick (UTM 758256 E., 3985463 N.).

Pliocene and Quaternary Deposits

In contrast to the Hualapai Limestone and the Muddy Creek Formation(?), the conformably overlying (lower Pliocene) deposits of Hualapai Wash (Tdh) include zircon grains that are indicative of a more distant Colorado Plateau provenance (Crossey and others, 2015; Kimbrough and others, 2015). The deposits of Hualapai Wash thus record an initial influx of far-traveled sediment. This event was interpreted as the arrival of Colorado River waters from the plateau, forming a delta plain into a lake basin floored by undissected strata of the Hualapai Limestone (Howard and Bohannon, 2001; Howard and others, 2008). The Colorado River presumably initially debouched westward from the Grand Wash Cliffs area into a shallow lake or lakes floored by the Hualapai Limestone and began entrenching after the lake(s) spilled farther downstream (see, for example, Spencer and others, 2013). The fine-grained and heterogeneous character of the deposits of Hualapai Wash is consistent with their deposition in an area sheltered from the major throughflow. The deposits of Hualapai Wash and the (overlying) lower Pliocene cemented alluvial conglomerate of White Elephant Wash (Tca) track a distance of about 15 km concordantly above the Hualapai Limestone. The White Elephant Wash unit marks a transition to dryland conditions following draining of the wetland delta plain, a transition inferred to be driven by entrenchment of the Colorado River system (see, for example, Schmidt and others, 1996).

Lower Pliocene ancestral Colorado River deposits, characterized by quartz-rich rounded sand and roundstone gravel and fluvial structures, are inset into the upper Miocene Hualapai Limestone and older units (fig. 5). The ancestral Colorado River deposits in Detrital Valley and some in Temple Basin are mapped as the Bullhead Alluvium (Trb, Trbg, Trbs). The Bullhead Alluvium (Howard and others, 2015) records a major aggradation all along the lower Colorado River valley from Lake Mead about 350 km south to Mexico, following initial river incision.

Some of the thin ancestral Colorado River deposits in Temple Basin reach an elevation of 700 m, which is near the top of the Hualapai Limestone. This level is similar to that of the lower Pliocene deposits of Hualapai Wash (Tdh) farther east, and it is higher than what is expected for the Bullhead Alluvium, which in Detrital Valley reaches a maximum elevation of 628 m. The stratigraphic position of these high ancestral-river deposits in Temple Basin is designated as uncertain, and they are mapped as

Figure 5. Crossbedded sandstone and roundstone conglomerate of the Bullhead Alluvium in Temple Basin. Southward-directed (to right) pebble imbrication, here and in Detrital Valley, is consistent with backfilling of tributary valleys during deposition of the Bullhead Alluvium in braidplains advancing southward away from axis of Colorado River valley. Hammer (circled) for scale (UTM 741647 E., 3985437 N.).

such (the river deposits of uncertain stratigraphic position; units Tr, Trg, Trs). The same designation applies to some thin sections of ancestral-river deposits elsewhere in Temple Basin and also 3 to 8 km east of Salt Spring Bay where they occupy the perched Spring Canyon paleovalley along the northern margin of this map area (Howard and others, 2003, 2008); the deposits typically rest on the limestone-block rubble (Tlr) formed by cliff collapse of undercut strata of the Hualapai Limestone. Where found at elevations higher than that of known Bullhead Alluvium, these river deposits of uncertain stratigraphic position are speculated to include pre–Bullhead Alluvium Colorado River deposits that were deposited and stranded as the river progressively incised from its initial floor on the Hualapai Limestone to a deeply entrenched valley that preceded Bullhead Alluvium aggradation. Paleosols on the highest patches in Temple Basin indicate long exposure.

The older alluvium (Ta) and the (overlying) old alluvium (QTa1) units record alluvial fans that postdate a new fall in base level caused by river entrenchment to the north; the fans progressed northward onto eroded deposits of the Bullhead Alluvium and older units. Calcrete soils (QTk) that are preserved on those and some older units record remnants of long-stable surfaces. The distribution of these surfaces that were stranded from younger erosion records the shape of late Pliocene to early Pleistocene landforms in the southwestern Temple Basin, as well as its west-bordering ridge of Mount Davis Volcanics and old alluvial fans on both sides of that ridge.

Structure and Mineralization

Foliations measured in gneiss by Duebendorfer and Sharp (1998), by this study, and by Blacet (1975) offer insight to both Proterozoic structure and Miocene deformation. Proterozoic foliation orientations were complex and were unlikely to be uniform over large areas. A pronounced bend and change in foliation orientations in the southern part of the "Lost Basin Range" may typify the expected complexities. However, Swaney and others (2010) and Umhoefer and others (2010b) pointed out that steep north-striking foliations south of this bend in uplifted footwall gneisses in the southern "Lost Basin Range" approximately parallel those 6 to 12 km southeast of the map area at Garnet Mountain (fig. 1*A*) where the gently dipping Cambrian Tapeats Sandstone overlies them (Blacet, 1975). The Garnet Mountain area is essentially not tilted and, thus, serves as a structural reference orientation to which the structure in other areas can be compared to assess post-Cambrian tilting. The foliations in the southern "Lost Basin Range" are consistent with being within 20° of, and possibly slightly east-tilted from, a pre-Miocene orientation similar to that of the Garnet Mountain reference. Gneiss in the hanging wall of the Salt Spring Fault west of Golden Rule Peak similarly exhibits steep pre-Miocene foliations that are subparallel to the Garnet Mountain reference orientation.

Gneissic foliations elsewhere in the "Lost Basin Range" and in two areas of the footwall of the Salt Spring Fault (one south of Golden Rule Peak and another about 5 km southeast of Salt Spring Bay) tend to lie within 20° to 50° from the Garnet Mountain reference orientation, patterns that could be consistent with being not tilted or modestly east-tilted from pre-Miocene Garnet Mountain–like orientations.

In contrast, more western areas of the footwall of the Salt Spring Fault have foliation maxima that are near horizontal, on the order of 90° shallower than at Garnet Mountain (see, for example, Duebendorfer and Sharp, 1998). This could reflect new Miocene transposition foliation related to the Salt Spring Fault, or regional pre-Miocene variations in fabric (such as shallower dip with greater depth), or extreme(?) tilting from Garnet Mountain–like orientations, or combinations of these. These measured outcrop foliations commonly dip less steeply than lithologic layering mapped (from remote sensing) as form lines along layers and pods of mafic and quartz-poor gneiss and leucogranitic gneiss. The form lines clearly show the broad, northwest-plunging synform mapped south of Salt Spring Bay. Duebendorfer and others (2010) interpreted more intricate, shallowly west- and east-plunging folds that Duebendorfer and Sharp (1998) mapped near Salt Spring Wash as products of the Miocene extensional deformation. Sense-of-shear indicators in mylonitic gneiss observed by Duebendorfer and Sharp (1998) near Salt Spring Wash, as well as during this study in two outcrops of gently dipping mylonitic garnet paragneiss (Xgr), 5 km east of Salt Spring Bay, are top-to-the-east, as observed in several nearby outcrops in the adjoining Hiller Mountains quadrangle (fig. 1*A*). This is opposite to the shear sense described for western parts of the Gold Butte block (Fryxell and others, 1992) or anticipated for westward slip on the Salt Spring Fault; instead, it is consistent with the possibility that the mylonitization predates and, thus, is not related to the detachment faulting (Duebendorfer and Sharp, 1998).

The sinuous Salt Spring Fault records many kilometers of Miocene extensional slip. Eastward dips of middle Miocene rocks in the hanging wall of the fault are taken to indicate that some parts of the fault are back-tilted eastward, along with its segmented hanging wall and parts of its footwall (Duebendorfer and Sharp, 1998). Some reentrant segments of the Salt Spring Fault, instead, dip gently to the north and are bordered by north-dipping Miocene strata; they were proposed to represent linkage of en echelon parts of the fault system (Duebendorfer and others, 2010). As the hanging wall moved mainly westward and tectonically unroofed the footwall, buoyancy allowed the footwall to warp upward isostatically (Duebendorfer and others, 2010).

The reentrants and intervening salients describe synforms and antiforms in the fault surface, shapes that are roughly reflected in the dissected, domelike footwall landscape (fig. 1*B*). A hanging-wall klippe or reentrant of Miocene conglomerate and breccia conceals the exposed footwall immediately south of the map area, near the boundary between R. 19 W. and R. 18 W. (Duebendorfer and others, 2010). Anderson and others (2013) mapped contractional structures in hanging-wall strata and suggested the sinuosity of the fault is a product of north-south-directed contractional folding of an originally more planar fault.

The footwall block of the South Virgin–White Hills Detachment Fault 20 km north of the map area, there known as the Gold Butte block (fig. 1*A*), rides on the Iceberg Canyon Fault and other gently west-dipping faults (Longwell, 1936; Brady and others, 2000). To indicate this geometry, our cross section portrays the footwall block as possibly being floored by the Iceberg Canyon Fault or a related west-dipping normal fault.

Thermochronologic studies in the footwall rocks record Miocene quenching of the Proterozoic rocks during structural unroofing and uplift of the Salt Spring Fault and the fault-block uplift of the "Lost Basin Range" (Fitzgerald and others, 2009). Miocene apatite fission-track dates become older eastward from the exposed Salt Spring Fault at a rate of about 1.1 to 1.2 km/m.y., which is interpreted as the slip rate of the fault (Fitzgerald and others, 2009).

The steeper Lost Basin Range Fault, which is part of the Wheeler Fault system, is marked by the sharply defined west front of the "Lost Basin Range" (fig. 1*A*). Its activity, which may have begun in the middle Miocene (Lucchitta, 1966; Umhoefer and others, 2010a), continued into the Pleistocene, as it cuts the old alluvium (QTa1). A hanging-wall rollover fold tilts the Hualapai Limestone (Th) and younger strata (Tdh, Tca) into eastward dips toward the fault. The tilting may affect a Pliocene paleovalley east of Salt Spring Bay that is marked by remnants of ancestral Colorado River gravel (Trg; Howard and others, 2003, 2008). Relations exposed north of the map area show that drag along the fault has modified the rollover into an asymmetric, north-striking syncline, here concealed (Howard and others, 2000; Wallace and others, 2005; Seixas and others, 2015).

Other gentle folds expressed in the Hualapai Limestone are superposed onto the Miocene extensional faults and their related stratal tilts. These late folds include a northward sag into Temple Basin and north-striking anticlines and synclines in Detrital Valley formed by either blind, down-to-the-west normal faulting or salt diapirism (or both) (Anderson and Laney, 1975).

The central part of the map area occupies the northern margin of a pronounced magnetic and gravity low in basement rocks (Langenheim and others, 2010). The lows suggest the presence of a subsurface nonmagnetic body, leading us to conjecture such a body at depth in our cross section. Late Cretaceous two-mica granite exposed in small areas south of the map area (Theodore and others, 1987) is a candidate for the nonmagnetic subsurface body.

Theodore and others (1987) extensively documented gold mineralization in and around the eastern parts of the map area. Those authors recovered visible gold at many sites, both in Proterozoic rock units and in young placer deposits, and they concluded that mineralization occurred in Proterozoic, Cretaceous, and Miocene times. They associated some mineralization with Miocene detachment faulting but interpreted much of the mineralization as being related to intrusion at depth of the Late Cretaceous two-mica granite.

Landscape Evolution

Buttress unconformities help record a Miocene basin-and-range landscape of eastward-tilted fault-block ridges. A middle Miocene stratigraphic record of rock avalanches, debris flows, gravel, and a kilometer-thick construct of Mount Davis Volcanics indicates how the basins that flank these tilt-block ranges partly filled and then underwent further faulting and tilting, along with other parts of the superdetachment basins above the Salt Spring Fault.

A dissected, westward-sloping domal highland that occupies the western part of the footwall of the Salt Spring Fault reflects that fault's upwarped shape. East-facing erosional scarp 3 (fig. 1*B*) interrupts this dissected dome. We attribute the scarp to erosion eating westward into the domal shape in response to incipient lowering and eastward-tilting of a half-graben basin in the hanging wall of the Lost Basin Fault. The scarp, which varies from 100 to 400 m high, locally consists of two steps, indicative of separate stages of backwasting. The Hualapai Limestone (Th) and locally present gypsiferous mudstone (Tmg) lap westward over a dissected surface toward the base of the erosional scarp. This relation leads to the inference that the scarp is older than those units. The scarp loses definition to the south near Golden Rule Peak where it crosses a southwestern salient of the footwall (fig. 1*B*). The salient marks a west-plunging antiformal shape of the fault (Duebendorfer and others, 2010).

The faulted ridges of mesa-forming olivine basalt (Tob) in the upper plate of the Salt Spring Fault form a highland that is elongated east-west but is segmented by dominantly north-striking faults and fault valleys. Irregular erosional scarps 1 and 2 (fig. 1*B*), each 100 m high or less, isolate this faulted series of basalt mesas. Younger olivine basalt (Tby) and underlying conglomerate (Tcl) postdate scarp 1, as they lap southward over where the olivine basalt (Tob) would project northward into the air. If the distribution of the perched olivine basalt represents topographic inversion of an original distribution, it would imply accumulation in an east-west-trending paleovalley before erosion (L.S. Beard, written commun., 2015). Alternatively, or in addition, mesa-bounding scarps commonly form the eroded faces of resistant strata that are flat or dip gently away from the scarp. If scarps 1 and 2 formed similarly, then the north-facing scarp 1 may have developed before the resistant olivine basalt (Tob) acquired its modern gentle northward dip toward Temple Basin. South-facing scarp 2 may have developed, or been enhanced, in response to northward tilting of the olivine basalt as the adjacent west-east-trending antiformal salient of the Salt Spring Fault was warped up.

Erosional scarp 4 marks where the resistant Mount Davis Volcanics form a protective cap over underlying sedimentary rocks in the hanging wall of the Salt Spring Fault. The scarp, as well as the Salt Spring Wash at its base, presumably migrate northwestward as erosion migrates down the dip of the Salt Spring Fault, progressively exposing the domal footwall of the fault.

Upper Miocene evaporites, mudstone, and limestone show that, as the basins filled with sediment, they became occupied by desiccating playas and lakes fed by mineral-rich spring waters (Crossey and others, 2015; Faulds and others, 2016). The Hualapai Limestone filled a paleovalley that bridged the highlands between Temple Basin and the Hualapai Wash area to the east (Faulds and others, 2008, their fig. 20; Howard and others, 2010). Arrival nearby of the newly integrated Colorado River signaled a major change in geomorphic regime from a Miocene time of interior basin filling to a Pliocene time governed by fluctuating base levels set by the river as it cycled between entrenchment and aggradation. Early Pliocene dissection and basin exhumation northward toward an incising river was followed by refilling of the basins by the Bullhead Alluvium, deposited in aggrading fluvial braidplains. Upland patches of calcrete (QTk; see also, fig. 3), old alluvium (QTa1), and older alluvium (Ta) mark remnants of subsequent landscapes that were graded to levels below the top of the Bullhead Alluvium. Those landscapes since have been dissected owing to river reentrenchment and degradation.

Interpreted Geologic History

Estimated ages are provided in brackets. Note that some of the numbered events overlap in age.

Proterozoic Time

1. Parent material of paragneiss, some mafic gneiss, and related rocks accumulate [prior to 1.7 Ga].
2. Mafic to leucocratic granitoids are intruded.
3. Metamorphism reaches upper-amphibolite to granulite(?) facies, and deformation fabric develops [1.8–1.7 Ga Yavapai-Ivanpah orogeny].
4. The Granite of Burro Spring (Yb) is intruded [about 1.4 Ga].
5. Diabase (Yd) dikes intrude [about 1.1 Ga].

Paleozoic Time

1. About 1.5 km of shallow-marine-platform and nearshore sediments accumulate [Cambrian to Permian].

Mesozoic Time

1. Shallow-marine, then continental, strata are deposited [Triassic and Jurassic].
2. Thick-skinned deformation forms the archlike Kingman Uplift [related to Sevier and (or) Laramide orogenic folding and thrusting].
3. Two-mica granite [Late Cretaceous] intrudes at depth, south of the map area (Theodore and others, 1987), potentially producing the large low-gravity and -magnetic anomalies (Langenheim and others, 2010).
4. Top-to-the-east mylonitization [Cretaceous(?)] (Duebendorfer and Sharp, 1998).
5. Undated [Mesozoic(?) or Proterozoic(?)] retrogressive metamorphism of the retrograded-garnet-bearing paragneisses (Xgp, Xgr).

Paleogene Erosion

1. Erosion strips the Paleozoic and Mesozoic cover strata from the Kingman Uplift (Bohannon, 1981) [Mesozoic to Paleogene].
2. Streams that drain northeastward across the region's highlands deposit rim gravels of the Music Mountain Formation (not preserved in the map area) onto the Colorado Plateau (Young and Hartman, 2014).

Miocene Extension and Basin Filling

1. Tectonic extension lowers and breaks up the Basin and Range Province, including the map area, relative to the Colorado Plateau to the east [17–14 Ma].
2. Down-to-the-west normal faulting, accompanied by eastward tilting on the major Salt Spring Fault and its numerous subsidiary hanging-wall normal faults, lead to accumulation and deformation of the sedimentary breccia and conglomerate (Tbc, Tbco) and megabreccia (Tbx), which were shed off faults and ridges into hanging-wall supradetachment basins [about 17–14.7 Ma] (Duebendorfer and Sharp, 1998).
3. Eruptions to the west emplace ash-flow tuffs [15.2–15 Ma].
4. The footwall rocks of the Salt Spring Fault, which may experience new greenschist-facies metamorphism, undergo major upwarping, tectonic and erosional denudation, and cooling [quenched apatite fission-track ages of about 18 to 13 Ma] (Fitzgerald and others, 2009; Verdel and others, 2011).
5. Progressive eastward unroofing, tilting, and warping of the Salt Spring Fault forms a domelike footwall landscape.
6. Mafic flows and associated conglomerate of the Mount Davis Volcanics accumulate thickly in the western and north-central parts of the map area during continued tilting [14.6–14 Ma]. The eruptive sequence transitions with time from pyroxene andesite (Tda) to olivine-pyroxene basalt (Tdo) while undergoing tilting and local erosion.
7. Continued normal faulting and extension forms a large upper-plate fault-block range of eastward-tilted Mount Davis Volcanics, which separates Temple Basin from Detrital Valley.
8. The lower conglomerate (Tcl) accumulates in the basins [14–10.8 Ma].
9. Eruptions of the olivine basalt (Tob) continue the igneous transition from intermediate-composition to more mafic volcanism [about 13–12 Ma].

10. Extensional faulting and eastward tilting wane and, finally [about 10 Ma], cease on the Salt Spring Fault and its hanging wall (Blythe and others, 2010), leaving a domed footwall, as well as a large, eastward-tilted fault block, which consists of rocks of the Mount Davis Volcanics, between Detrital Wash from Temple Basin.
11. Warping along an east-striking axis tilts the footwall and hanging wall of the north side of the Golden Rule Peak salient of the Salt Spring Fault northward.
12. Erosional scarp retreat isolates the resistant olivine basalt (Tob) in faulted mesas between north- and south-facing scarps 1 and 2, respectively.
13. The young olivine basalt (Tby) erupts and spreads in Temple Basin [about 11–8.4 Ma].
14. Halite, gypsum, and mudstone accumulate as interior basins continue to fill while gradients and clastic-sediment supply decrease and spring-fed lakes intermittently go dry [about 9–7 Ma].
15. The upper conglomerate (Tcu) accumulates [about 8.4–7 Ma].
16. Faulting on the Lost Basin Range Fault continues to raise the "Lost Basin Range" and to lower and tilt a hanging-wall half graben on its west side.
17. Westward erosion up the dip slope from the hanging-wall half graben into the domal footwall of the Salt Spring Fault develops east-facing erosional scarp 3 and causes it to retreat westward [between 14 and 6 Ma].
18. Continued influx of spring-fed water into lake(s) and wetlands, and their intermittent drying, results in the deposition of gypsum that interfingers with mudstone (Tmg, Tm) and overlying limestone (Th) over the upper conglomerate (Tcu) [about 9–6 Ma] (Crossey and others, 2015). The host lake connects the Hualapai Wash basin and Temple Basin, and it deposits the Hualapai Limestone (Th) in interbasin passes across shoaling highlands.
19. Temple Basin continues to sag, causing rocks as young as the Hualapai Limestone to dip gently northward.
20. Down-to-the west, blind normal faulting and salt diapirism cause folding in Detrital Valley [about 6–4 Ma].

Pliocene Aggradation-Incision Cycles Following Arrival of Colorado River

1. The deposits of Hualapai Wash (Tdh) accumulate as the first-arriving sediments delivered from the Colorado Plateau by ancestral Colorado River(?) waters, spreading thinly in distal part of a delta plain onto a floor of the Hualapai Limestone [between 6 and 5.3 Ma].
2. Alluvial fans deposit the cemented alluvial conglomerate of White Elephant Wash (Tca) over the deposits of Hualapai Wash (Tdh), possibly as the river entrenches itself north of the map area, thereby draining and then stranding the delta-plain deposits and exposing the former delta plain to encroaching alluvial fans.
3. Regional degradation caused by ancestral Colorado River entrenchment causes erosion into the Hualapai Limestone (Th) and the underlying mudstone (Tm) of the Muddy Creek Formation(?), thereby undermining limestone mesas that collapse to form the limestone-block rubble (Tlr).
4. River incision north of the map area [about 5.3–4.5 Ma] causes regional degradation, possibly in a staggered fashion that deposits and then strands some ancestral Colorado River deposits (Tr, Trg, Trs) onto the limestone-block rubble (Tlr).
5. The degradation exhumes Miocene basins.
6. Faulting on the Lost Basin Fault continues to tilt the hanging-wall strata eastward, tilting units as young as the cemented alluvial conglomerate of White Elephant Wash (Tca), and likely the ancestral Colorado River sediments (Trg) that mark a paleovalley in Spring Canyon.
7. Major Colorado River aggradation backfills southward as wide braidplains that extend into Temple Basin and Detrital Valley. These braidplains refill the exhumed Temple Basin and

Detrital Valley with thick deposits of the Bullhead Alluvium (Trb, Trbg, Trbs), which contain southward-directed current imbrication up these tributary paleovalleys [about 4.5–3.5 Ma].

8. Continued faulting in Detrital Valley locally folds the Bullhead Alluvium, and it also contributes to 200 m of inferred net fault uplift of the Bullhead Alluvium and its substrates relative to the western Lake Mead area (fig. 1*A*) (Howard and others, 2015).
9. Colorado River reentrenchment north of the map area causes degradation and leads to the older alluvium (Ta) in Pliocene alluvial fans progressing northward over the eroded Bullhead Alluvium.
10. Further fall in base level dissects and strands mesas of the older alluvium (Ta) and remnants of calcrete soils (QTk) while accumulating the old alluvium (QTa1) in inset fans [Pliocene and Pleistocene].
11. As erosion continues, the intermediate-age alluvium (Qa2), the younger alluvium (Qa3), and the youngest alluvium (Qa4) accumulate in successively more inset fans [Pleistocene to Holocene].

DESCRIPTION OF MAP UNITS

SEDIMENTARY AND VOLCANIC ROCKS AND DEPOSITS

Qt **Talus deposits (Quaternary)**—Basalt blocks on talus slopes

Ql **Landslide and colluvium deposits (Quaternary)**

Piedmont alluvium

Qa4 **Youngest alluvium (Holocene)**—Angular gravel and sand, in active washes. As much as 1 m thick

Qa3 **Younger alluvium (Holocene)**—Piedmont alluvial and alluvial fan deposits of angular gravel and sandy gravel. Bar-and-swale landforms well expressed. Minor soil development. As much as 2 m thick

Qa2 **Intermediate-age alluvium (Pleistocene**)—Piedmont alluvial and alluvial fan deposits of angular gravel and sandy gravel, in low terraces. Soil development includes eolian-derived addition and translocation of reddish silt; some carbonate rinds on pebbles. Surfaced by desert pavements of varnished stones. Pebbly desert pavements locally (SW¼SW¼ sec. 28, T. 30 N., R. 19 W.) exhibit multiple contouring stripes about 0.5 m wide of unvarnished, finer grained grit, interpreted as sheetwash features. In Detrital Valley, locally dominated by reworked roundstone pebbles exhibiting imbrication directed downstream in modern landscape. As much as 2 m thick

Erosional Unconformity

QTk **Calcrete (Pleistocene and Pliocene)**—Calcitic soil (stage IV to VI), typically developed on old alluvial fan surfaces of the old alluvium (QTa1), the older alluvium (Ta), locally on the Bullhead Alluvium (Trb, Trbs), and on eroded surfaces of mafic flows (for example, the basaltic andesite, Tda). Surface littered by light-toned calcitic fragments; calcite rinds on clasts are several centimeters thick. As much as 2 m thick

Old piedmont alluvial deposits

QTa1 **Old alluvium (Pleistocene and Pliocene)**—Alluvial fan deposits of gravel and sandy gravel. Clasts largely angular but locally include roundstones derived from the ancestral Colorado River deposits. In Temple Basin and Detrital Valley, commonly contains basalt and andesite boulders; locally in Temple Basin, includes rare limestone blocks 1 to 3 m across derived from the Hualapai Limestone. Typically poorly to moderately well consolidated, dissected into ridge-and-ravine landscape. Extensive soil development; carbonate soil, mostly stage III to IV; surface where undissected commonly appears spotted on aerial images by patches of calcrete litter. Cemented on east side of Temple Wash drainage in north-central part of map area. Locally forms cliffs. As much as 12 m or more thick. Overlies the older alluvium (Ta) in Temple Basin; is inset into eroded terraces of the older alluvium (Ta) in Detrital Valley. Likely represents more than one alluvial fan sequence in which younger deposits are inset into older ones. Cemented exposures east of Temple Wash may include correlatives of the cemented alluvial conglomerate of White Elephant Wash (Tca) or of the older alluvium (Ta)

Ta **Older alluvium (Pliocene)**—Largely angular-clast, poorly sorted, sandy-gravel alluvial-fan deposits of local derivation. Locally contains roundstones reworked from gravels of the ancestral Colorado River deposits. In Detrital Valley, includes pale-orangish-gray mud and sand that contains rounded quartz sand grains; angular, grit-size gneiss grains; and rare rounded quartzite pebbles. Deeply dissected to ridge-and-ravine landscape in Temple Basin, but remnant high, undissected terraces on east side of Detrital Valley slope toward valley and project above highest exposures of the Bullhead Alluvium. More than 6 m thick. Exhibits calcareous paleosol more than 2 m thick (stage IV to V), generally mapped as calcrete unit (QTk), indicative of long exposure. Thickness, as much as 24 m or more. Overlies the Bullhead Alluvium (UTM 3982300 N., 731800 E.) and other sediments of the ancestral Colorado River deposits on erosional unconformity. Contacts with the old alluvium (QTa1) and the conglomerate (Tc) are commonly indistinct, poorly defined, and uncertain

Erosional Unconformity

Ancestral Colorado River deposits (lower Pliocene)—Moderately well cemented, well-sorted, quartz-rich sand, pebbly sand, and matrix- and clast-supported roundstone gravel. Erosionally inset into the Hualapai Limestone and other units. Advanced carbonate soil preserved on relict surfaces

Bullhead Alluvium—In Detrital Valley, is 100 m thick, overlies the mudstone (Tm) on angular unconformity, and is interpreted as upper part of a thick (more than 200 m) aggraded fluvial accumulation. Also includes 15-m-thick section in Temple Basin (fig. 5). Current directions measured from pebble imbrication and sand crossbedding mostly directed upvalley away from modern Colorado River. Outcrop photographs available in Howard and others (2015)

Trb **Bullhead Alluvium, undivided**

Trbs **Sand**—Coarse to fine, quartz-rich, cross-stratified sandstone, pebbly sandstone, and lesser amount of rounded gravel and conglomerate. Contains rounded quartz grains. Includes uncemented, loose sand that is subject to redistribution by wind. Exhibits planar- to trough-crossbedded, northwest-dipping pebbly-sand crossbeds as high as 2 m, in southern exposures in Detrital Valley. Contains thin beds of reddish-brown siltstone. As much as 40 m thick

Trbg **Gravel**—Moderately to well sorted roundstone gravel and conglomerate; varies from sandy-matrix supported to clast supported. Characterized by well-rounded pebbles of black chert and pebbles and cobbles of quartzite and Paleozoic limestone. Clast assemblage also includes volcanic rocks, gneiss, rare red sandstone and jasper, and (near base on the Hualapai Limestone) algal-limestone blocks. Sandstone lenses; rarer interbeds of locally derived angular debris

River deposits of uncertain stratigraphic position—Moderately well cemented roundstone gravel and sand; indistinguishable lithologically from the Bullhead Alluvium. Exposures that are higher than 2,000 ft (610 m) elevation in Temple Basin are capped by more than 2-m-thick, pale-orangish-gray, calcareous paleosol that contains mix of small, rounded pebbles and grains and angular, locally derived clasts. In Temple Basin, is found to elevations as high (700 m) as uppermost exposures of the Hualapai Limestone. Also occupies Spring Canyon paleovalley east of Salt Spring Bay (Howard and others, 2008). Commonly rests on the limestone-block rubble (Tlr). May include the Bullhead Alluvium, but correlation uncertain owing to thinness, to some unusually high-elevation exposures in Temple Basin, and to occurrences of uncertain stratigraphic position in Spring Canyon paleovalley. May include pre-Bullhead Alluvium deposits laid down and stranded during pauses in intermittent pre-Bullhead Alluvium entrenchment into the Hualapai Limestone by ancestral Colorado River, possibly analogous in concept to the regrade gravel of Moapa unit (Schmidt, 1994; Swadley and others, 1995; Schmidt and others, 1996) mapped and interpreted north of Lake Mead

Tr **River deposits, undivided**—Rests locally on calcareous paleosol over rocks of the Mount Davis Volcanics

Trs **Sand**—Quartz-rich sand that includes rounded quartz grains; rare roundstone pebbles

Trg **Gravel**—Roundstone gravel and conglomerate. In Spring Canyon paleovalley east of Salt Spring Bay, is as thick as 60 m; contains rare petrified wood; lower part contains 0.4-m-wide rounded boulder of silicic volcanic rock, locally derived subrounded to angular boulders as large as 1 to 2 m of porphyritic granite and gneiss, and limestone blocks as large as 5 m derived from the Hualapai Limestone; measured current imbrications directed eastward and westward; cut by steep, north-striking travertine vein; possibly includes roundstone gravel reworked by local streams

Tlr **Limestone-block rubble (lower Pliocene)**—Blocks derived from the Hualapai Limestone. Blocks typically 0.5 m to 4 m across and locally as wide as 20 m (northeasternmost exposure). Rare angular gneiss blocks. Rare interstitial roundstone-pebble gravel. Locally (5 km east of Salt Spring Bay), rubble overlies basal, poorly sorted, angular gneiss-clast conglomerate that exhibits westward-directed (upslope now) clast imbrication (UTM 3986790 N., 753128 E.). Overlies the mudstone (Tm) of the Muddy Creek Formation(?) and the undivided conglomerate (Tc). Underlies the ancestral Colorado River deposits. Interpreted as formed where eroding limestone cliffs collapsed, broke, and slid on underlying or interbedded mudstone and gypsum during regional degradation

Erosional Unconformity

Tca **Cemented alluvial conglomerate of White Elephant Wash (lower Pliocene)**—Poorly sorted, angular conglomerate. Forms cliffy outcrops. Near Hualapai Wash in eastern part of map area. Poor clast imbrication is west directed where observed, in opposite sense to gentle eastward dip of unit. Thickness, 5 to 10 m. Concordantly overlies the (eastward-tilted) deposits of Hualapai Wash in map area, but, north of map area, contact locally is angular unconformity. Cosmogenic burial age modeled as 5.35+1.65/−0.97 Ma, assuming similar depositional ages for clast sampled from eroded upper surface of deposit and sample collected 6 m lower, from top of the (underlying) deposits of Hualapai Wash (Tdh) (Matmon and others, 2012). Interpreted as product of alluvial fans that aggraded over the deposits of Hualapai Wash after they were drained owing to river entrenchment north of map area. May correlate in process and, roughly, in time to the aggradational gravel of Whitmore Mesa unit, discussed and interpreted (Schmidt, 1994; Swadley and others, 1995; Schmidt and others, 1996) from Moapa, Nevada, area north of Lake Mead

Tdh **Deposits of Hualapai Wash (lower Pliocene)**—Very pale, orangish-gray silt; massive mudstone; very pale gray to greenish clay; sandy, angular diamictite; quartz-rich sand and laminated siltstone (pale gray to pale orangish gray); massive subangular sandstone; and very rare clay balls and well-rounded pebbles of fossiliferous limestone, quartzite, red chert, black chert, and volcanic rocks. Mudstone contains selenite crystals. Clay contains gastropods. Includes white limestone layer 3 m thick in northeastern part of map area (UTM 758664 E., 3985526 N.). Upper part contains interfingered, poorly sorted, angular pebbly sand. Compared to the Bullhead Alluvium and other ancestral Colorado River deposits (unit Tr), unit is finer grained and commonly more angular; in addition, extralocal roundstone pebbles and quartz-rich fluvial sand are much rarer. Detrital-zircon population (1 sample, 56 grains) resembles that of most other Colorado River deposits but lacks Paleozoic grains, similar to a sample of the (possibly correlative) Bouse Formation (Kimbrough and others, 2015). Exposed thickness, 10 to 15 m; subsurface thicknesses may be greater (table 1). Dips gently eastward and underlies the cemented alluvial conglomerate of White Elephant Wash (Tca) with little or no angular relation. Overlies the Hualapai Limestone with no angular relation. Interpreted as wetland delta-plain deposits that include far-traveled fluvial sand and pebbles delivered from Colorado Plateau before Colorado River entrenched into the Hualapai Limestone

Th **Hualapai Limestone (upper Miocene)**—Limestone and some interbedded orangish-gray mudstone and gypsiferous mudstone, minor reddish sandstone, local angular pebbles, gypsum, and rare biotite-vitric tephra layers. Color, gray to pink. Limestone locally contains one or more of the following structures: pisolites; reed impressions; planar to gently domal to wave-form stromatolite laminations, mounds, and dimples (fig. 4*B*); chert seams and nodules; intraformational boudins (fig. 4*A*); and related sag structures into pull-apart fractures. Contains diatoms, gastropods, ostracodes, and trace fossils attributed to wasps (Blair and Armstrong, 1979). Chert is more common westward; contains well-preserved diatoms pictured by Blair (1978); white-chert detritus from bed in Detrital Wash shows evidence of prehistoric working by humans (UTM 731506 E., 3983183 N.). Thickness, as much as 134 m in northwestern, and more than 122 m in northeastern, parts of map area. Crossey and others (2015) presented stratigraphic sections and isotopic chemostratigraphy for unit. Tephra interbed 40 m below top of formation on west side of Temple Basin (in unsurveyed sec. 22, T. 30 N., R. 20 W.) was dated as 5.97±0.07 Ma (biotite, $^{40}Ar/^{39}Ar$; Spencer and others, 2001); 24 m below this dated tephra, another tephra correlates with tephra in the Hualapai Limestone in Detrital Valley (Pearce and others, 2011). At locality 6 to 12 km north of map area in Temple Basin (where formation includes lower members not recognized in map area), tephra beds in formation were chemically correlated to tephras bracketed in age as 6.2 to 7.0±0.5 Ma, 6.27 to 7.5 Ma, and 9 to 10(?) Ma (Howard and others, 2010)

Muddy Creek Formation(?) (upper Miocene)—Tentatively correlated lithologically to the Muddy Creek Formation more than 50 km north of western part of map area, in area of Overton Arm of Lake Mead (in Nevada) and in Mesquite basin, near town of Mesquite, Nevada, northeast of Overton Arm (fig. 1*A*); there, formation is shown (Dickinson and others, 2014) to be of overlapping and younger age (that is, partly younger than the Hualapai Limestone; Dickinson and others, 2014), compared to age in map area. Although paleogeographic connections between depositional basins are uncertain, unit in Detrital Valley (in map area) is along structural strike with Overton Arm depositional basin for the Muddy Creek Formation

Tm **Mudstone**—Pale-orangish-gray to pale-yellowish-gray, poorly consolidated, bedded mudstone, siltstone, fine sandstone, and rare limestone; rare angular gravel and granite boulders at base. Some sand is rounded. Selenite crystals locally on surface. Locally contains vertebrates (remains of canid and smaller mammal were observed in Temple Basin; canid identified by R. Reynolds, written commun., 2000)

Tmg **Gypsum**—White to pale-orangish-gray gypsum and gypsiferous mudstone. Folded and faulted. Found in northwestern and, locally, southeastern parts of map area. Tephra layer in unit 10 km north of western part of map area was chemically correlated to tephra bed in the Hualapai Limestone north of central part of map area; both were correlated to tephra bracketed in age to between 6.27 and 7.5 Ma (Howard and others, 2010)

Tc **Conglomerate, undivided (upper and middle Miocene)**—Poorly to moderately sorted, nonmarine, angular conglomerate and sandstone of local derivation. East of Salt Spring Bay, is locally red and contains boulders of porphyritic granite and garnet paragneiss. Alluvial fan deposits. Blythe (2005) and Blythe and others (2010) detailed sedimentology and sedimentary structures, and they dated unmapped tephras near Salt Spring Bay. Cut by Salt Spring Fault near 36° N,, 114°15’ W.; unconformably overlies the (more steeply dipping) lower conglomerate (Tcl); is judged as lower in stratigraphic position than the upper conglomerate (Tcu), which elsewhere lies across Salt Spring Fault. Locally, subdivided into:

Tcu **Upper conglomerate (upper Miocene)**—Poorly sorted, locally derived conglomerate and sandstone. Clasts are dominantly gneiss, locally including retrograded-garnet gneiss. Includes sandstone that fills swales on top of the young olivine basalt (Tby). Well cemented where unit underlies the Hualapai Limestone; elsewhere, poorly cemented. Cut by calcite-filled faults near center of map area. Deposited across Salt Spring Fault

Tcl **Lower conglomerate (upper and middle Miocene)**—Poorly sorted, locally derived, angular to subangular conglomerate. Includes angular diamictite characterized by clasts of retrograded-garnet gneiss (UTM 747400 E., 3978700 N.). Dominantly westward-directed current and provenance indicators near Salt Spring Wash (Blythe and others, 2010; Howard and others, 2010). Includes coarse monomict debris-flow deposit in tributary of Salt Spring Wash (UTM 3978500 N., 747400 E.). In fault contact with older Miocene rocks and with gneiss on splay of Salt Spring Fault. Underlies the young olivine basalt (Tby). Unmapped tephra beds dated as 14.5 Ma and

13.1±0.5 Ma in map area and 10.8±0.4 Ma 1 km north of map area (^{40}Ar/^{39}Ar; Blythe and others, 2010). In angularly unconformable contact with the (overlying) undivided conglomerate (Tc) at Salt Spring Bay, which also is deformed, unlike most of the upper conglomerate (Tcu). Overlies, and reportedly interfingers locally with, the basaltic andesite (Tda) (Blythe and others, 2010). Overlies the undivided sedimentary breccia and conglomerate (Tbc), the old conglomerate (Tbco), and the megabreccia (Tbx) units on angular unconformity

Tct **Tephra bed(s) (Miocene)**—Reworked sandy, biotite-vitric volcanic ash. Thickness, 1 to 2 m. Interbedded with the lower conglomerate (Tcl). Mapped bed along east side of Salt Spring Wash, near center of map area, tentatively correlated chemically to tephra dated as 12.1 Ma (Howard and others, 2010)

Tby **Young olivine basalt (upper Miocene)**—Includes two to three vesicular flows near north border of map area, as well as conglomerate interbed as thick as 20 m. Olivine, plagioclase phenocrysts. Felted to intergranular texture. Calcite amygdules. Includes flow breccia. Crossed by steep calcite veins and minor faults in Temple Basin. Thickness, as much as 40 m. Preliminary age, 8.4 Ma, reported from 3 km north of map area (Beard and others, 2007; ^{40}Ar/^{39}Ar, Howard and others, 2010). Basalt dated as 10.9±0.6 Ma (K-Ar, using old constants; Blair, 1978) was reported as second flow below the Hualapai Limestone by Theodore and others (1987). Note that Blair's (1978) sketch map placed locality at about UTM 744800 E., 3985500 N., which is judged herein to be more likely than locality about 1.5 km to northwest that was specified by Theodore and others (1987). Included in the basalt of Senator Mountain by Cascadden (1991), for which 9.9-Ma ^{40}Ar/^{39}Ar age was determined near Senator Mountain 3 to 4 km south of map area (Faulds and others, 2010)

Tob **Olivine basalt (middle Miocene)**—Olivine-phyric to olivine-clinopyroxene-phyric. Multiple flow units. Forms prominent mesas in south-central part of map area (mapped as the basalt of Pink/Black Ridge by Cascadden, 1991). May include small angular unconformity between lower and higher stacks of flows. Thickness, as much as 120 m. Dated as 12.7±0.2 and 12.6±0.2 Ma at two sites in south-central part of map area (^{40}Ar/^{39}Ar, E.M. Duebendorfer, written commun., 2008). These ages suggest correlation with upper parts of the Mount Davis Volcanics (Anderson, 1971; Felger and others, 2014)

Tbi **Intrusive basalt (Miocene)**—Small intrusive bodies near center of map area and near Salt Spring Wash

Angular Unconformity

Mount Davis Volcanics (middle Miocene)—Includes local angular unconformities

Tda **Basaltic andesite**—Dark, massive flows and flow breccia of andesitic trachybasalt, trachyandesite, andesite, basaltic andesite, and andesitic basalt. Contains phenocrysts of plagioclase, clinopyroxene, and, locally, olivine. Upper part includes pyroxene-olivine basalt (locally, mapped separately as the olivine-pyroxene basalt [Tdo]). Includes dikes (Cascadden, 1991, p. 35, 57). See Cascadden (1991) for subdivision, geochemical characterization, and mapping as multiple subunits. Erosional and angular unconformities present within unit. Southwest of Squaw Peak, outcrop locally exhibits popcornlike secondary calcite crusts. Thickness, as much as 1 km. Within map area, dated as 14.6 Ma (whole rock, $^{40}Ar/^{39}Ar$, Duebendorfer and Sharp, 1998) and 14.7 Ma (whole rock, $^{40}Ar/^{39}Ar$, Beard and others, 2007; Howard and others, 2010). Overlies, and interfingers with, the undivided sedimentary breccia and conglomerate (Tbc) and the megabreccia (Tbx). Interfingers with the volcanic-clast conglomerate (Tdc). Queried southwesternmost outcrops, alternatively, may underlie the welded tuff (Twt) and may correlate to the (about 16-Ma) volcanics of southern White Hills of Faulds and others (2008, 2010), as compiled by Beard and others (2011). Locally, subdivided into:

Tdo **Olivine-pyroxene basalt**—Olivine-clinopyroxene-phyric basalt and interlayered basaltic andesite, in northern-central part of map area, as well as east of Squaw Peak and in northwestern part of map area. Locally, columnar jointed. May include interlayers of basaltic andesite. At Squaw Peak, rests in slight angular unconformity on the (underlying) basaltic andesite (Tda). In northwestern part of map area, red color and high vesicularity suggest near-vent facies

Tdc **Volcanic-clast conglomerate**—Poorly sorted, pale-orangish-gray to tan, angular pebble-to-boulder conglomerate and reddish coarse sandstone, locally arkosic. Clasts largely derived from basaltic andesite flows and scoria (similar to unit Tda) as well as some from gneiss. In southwestern part of map area, includes red conglomerate containing clasts of chloritic gneiss. Interfingers with, and overlies, the basaltic andesite (Tda). Thickest exposed section (180 m) near northwest corner of map area includes more than eight beds of light-toned tephra and pumice; sandwiched on angular unconformities between flows of the basaltic andesite (Tda)

Local Angular Unconformity

Tbc **Sedimentary breccia and conglomerate, undivided (middle Miocene)**—Includes megabreccia sheets 200 m thick and more than 1 km long, as well as debris-flow deposits near lower Salt Spring Wash (Duebendorfer and Sharp, 1998; Faulds and others, 2008; E. Duebendorfer, written commun., 2015). Clasts near Salt Spring Wash derived from gneiss, porphyritic granite (similar to unit Yb), and welded tuff (similar to unit Twt). As thick as 500 m or more. Correlated to the Thumb Member of the Horse Spring Formation north of Lake Mead (figs. 1*A*, 2; see also, Beard and others, 2007). Locally, divided into:

Tbco **Old conglomerate**—Poorly sorted, matrix-supported, pebble-to-cobble, gneiss-clast conglomerate. Red in places. Clast assemblage includes fresh-garnet gneiss (similar to unit Xgg) and basaltic andesite (similar to unit Tda)

Tbx **Megabreccia**—Consolidated breccia and megabreccia. In south-central part of map area, contains crackle breccia and clasts larger than 5 m of coarse-grained porphyritic granite (resembles the porphyritic monzogranite of Garnet Mountain of Theodore and others, 1987) that contains pink potassium-feldspar laths as long as 2 cm and also scattered quartz eyes; includes breccia of gneiss and quartzite clasts on west side of Salt Spring Wash. In south-central part of map area, includes clasts of garnet gneiss (similar to unit Xgg) and garnet-retrograded gneiss (similar to unit Xgr). In southwestern part of map area, includes clasts of garnet gneiss (similar to unit Xgg) and partly retrograded garnet gneiss (similar to unit Xgp), as well as of amphibolite and quartz diorite

Twt **Welded tuff (middle Miocene)**—Rhyodacitic welded tuff; contains sanidine and biotite crystals. Sphene content as much as 0.5 percent for eastern (apparently upper) tuff near Salt Spring Wash; elsewhere, sphene absent or only present in trace amounts (Cascadden, 1991). In Detrital Valley, varies from lithic-rich to crystal-rich (sanidine, plagioclase, biotite); as much as 122 m thick, according to Cascadden (1991). In Temple Basin, lithic-rich; contains fiamme as much as 10 cm long; contains sanidine and biotite crystals and some sphene; dated as 16.4±0.5 Ma (biotite, K-Ar, Cascadden, 1991) and 14.88±0.06 Ma (^{40}Ar/^{39}Ar, Howard and others, 2010); thickness of as much as 150 m includes two flow units, according to Cascadden (1991). In Salt Spring Wash area, found as two tuffs that are separated by and underlain by the undivided sedimentary breccia and conglomerate (Tbc). Eastern (apparently upper) exposure of tuff is lithic rich, crystal poor, white; 40 to 50 m thick (see photograph in Faulds and others, 2008, their fig. 17); dated as 15.2 Ma (sanidine, ^{40}Ar/^{39}Ar); said to be isotopically distinct from the tuff of Bridge Spring (Duebendorfer and Sharp, 1998; see also, Anderson, 1971). Western (lower) exposure of tuff is crystal rich (sanidine, biotite); contains 1-cm-long fiamme, some lithic fragments, and no sphene; about 50 m thick; additional small outcrops (not mapped herein) were mapped by Anderson and others (2013). Correlated to either or both of two ignimbrites in Black Mountains (fig. 1*A*), dated as 15.0 and 15.2 Ma, respectively (Faulds and others, 1995, 2002): namely, the tuff of Mount Davis (Faulds and others, 1995, 2002) and the tuff of Bridge Spring (Anderson, 1971)

TXbrk **Breccia, conglomerate, granite, and gneiss, undivided (Miocene and Proterozoic)**—Mapped in poorly exposed areas in upper plate of Salt Spring Fault, where contacts are indistinct between Miocene sedimentary rocks and Proterozoic bedrock. Includes reddish, crackle-brecciated, medium-grained biotite granite

Nonconformity Below Miocene Rocks

ANCIENT INTRUSIVE AND METAMORPHIC ROCKS

Yd **Diabase (Mesoproterozoic)**—Forms small dike or sheet intrusion, in south-central part of map area near Salt Spring Wash. Texture, ophitic

Yb **Granite of Burro Spring (Mesoproterozoic)**—Porphyritic biotite granite and granodiorite that contains potassium-feldspar phenocrysts as long as 1.3 cm. Contains oblate mafic enclaves and disoriented xenoliths of banded gneiss. Exhibits crosscutting biotite pegmatite dikes. Zone as much as 0.5 km wide that borders host gneiss lacks phenocrysts, and it also is foliated and lineated parallel to fabric in host gneiss. In northeastern part of map area. Correlated lithologically with the Gold Butte Granite in the southern Virgin and Hiller Mountains (fig. 1*A*) (Longwell, 1936; Fryxell and others, 1992; Howard and others, 2003). Blacet (1975) suggested correlation with the monzogranite of Garnet Mountain of Theodore and others (1987), which is Paleoproterozoic; however, unit lacks discrete quartz that is characteristic of that unit; instead, lithology of unit closely resembles that of the Gold Butte Granite (dated [U-Pb] as 1,372±12 Ma; Crossey and others, 2015)

Xhl **Leucogranite of Greggs Hideout (Paleoproterozoic)**—Medium-grained to sparsely porphyritic leucogranite. Contains discrete quartz and altered biotite (Blacet, 1975; Howard and others, 2003). Borders against gneiss units are mylonitic to ultramylonitic. Exhibits hematite-stained fractures

Xg **Gneiss, undivided (Paleoproterozoic)**—Dark, psammitic to pelitic paragneiss; leucogranite to granodiorite gneiss; migmatite; pegmatite; mafic gneiss; and amphibolite. Includes small amounts of marble, skarn, metaquartzite, metamorphosed banded-iron formation, and metachert (Theodore and others, 1987). In "Lost Basin Range," includes fine-grained quartz-feldspar gneiss; locally, calc-schist and marble; kyanite-biotite schist, and sillimanite-, cordierite-, and hercynite-bearing gneisses (Theodore and others, 1987). Near southeast corner of map area, in "Lost Basin Range," includes massive to layered, strongly lineated gneiss (map unit "fgn" of Blacet, 1975). Prograde upper-amphibolite-facies mineral assemblages, variably retrograded to lower degrees of metamorphism (Theodore and others, 1987). Highly chloritized and disrupted or brecciated adjacent to overriding Salt Spring Fault (Duebendorfer and Sharp, 1998). Locally, subdivided into:

Xgm **Mafic and quartz-poor gneiss**—Mafic gneiss, amphibolite, metadiorite, and quartz-poor gneiss. Mapped largely from interpretation of MODIS/ASTER Airborne Simulator (MASTER) multispectral imagery (see, for example, Hook and others, 2005). Orthopyroxene absent (Theodore and others, 1987). Locally (near southeast corner of map area), includes calc-silicate rocks. Partly chloritic, even locally where biotite is fresh

Xgl **Leucogranitic gneiss**—Mapped largely from aerial photographs. Includes migmatitic alaskite mapped by Blacet (1975)

Xgg **Paragneiss, garnet fresh**—Dark, semipelitic quartz-plagioclase-garnet-biotite gneiss and some garnet leucogranite gneiss. East of Salt Spring Bay, includes brecciated, Miocene(?) biotite-phyric rhyodacite dikes not mapped separately

Xgp **Paragneiss, garnet partly retrograded**—Dark, semipelitic quartzofeldspathic gneiss; locally, amphibolite and garnet-bearing leucogranite gneiss. Garnet partly replaced by chlorite and mica assemblages

Xgr **Paragneiss, garnet retrograded**—Dark, semipelitic quartzofeldspathic gneiss and some leucogranite gneiss. Garnet replaced by chloritic and micaceous pseudomorphs or (near the granite of Burro Spring [Yb]) by biotite pseudomorphs. Well lineated and mylonitic, 3 to 5 km east of Salt Spring Bay. On basis of its presence in northern and southwestern exposures of footwall of Salt Spring Fault, western (left) part of cross section (on map sheet) notes that some of this Xgr lithotype is expected at depth in footwall, mixed with the undivided gneiss (Xg)

Acknowledgments

Ernie Duebendorfer and Mel Kuntz expertly introduced one of us (Keith Howard) to the complex geology of the area. We also thank Ernie Anderson, Dwight Schmidt (1926–2007), Jim Faulds, and Sue Beard for sharing further regional perspectives. Dwight suggested interpretations for the deposits of Hualapai Wash, the cemented alluvial conglomerate of White Elephant Wash, and the limestone-block rubble units. Bob Reynolds gave expert opinions on sedimentary structures and a fossil. We are grateful to many scientists whose cited previous work is used and generalized in the map. We thank Simon Hook for sharing MASTER imagery, and Ernie Duebendorfer for sharing his unpublished dating results done with Warren Sharp. We thank Zack Anderson, Linda Howard, Crystal Tolentino, and Chris Cox for field assistance, and Debra Block for the final digital preparation and digital review. Sue Beard and Ernie Duebendorfer provided careful expert reviews that improved the map, cross section, and text.

References Cited

Anderson, R.E., 1971, Thin skin distension in Tertiary rocks of southeastern Nevada: Geological Society of America Bulletin, v. 82, p. 43–58.

Anderson, R.E., 1977, Geologic map of the Black Canyon 15′ quadrangle, Mohave County, Arizona and Clark County, Nevada: U.S. Geological Survey Geologic Quadrangle Map GQ–1394, scale 1:62,500.

Anderson, R.E., Beard, L.S., Mankinen, E.A., and Hillhouse, J.W., 2013, Analysis of Neogene deformation between Beaver, Utah, and Barstow, California—Suggestions for altering the extensional paradigm, *in* Anderson, E.A., ed., Neogene deformation between central Utah and the Mojave Desert: Geological Society of America Special Paper 499, p. 1–67, doi:10.1130/2013.2499(01).

Anderson, R.E., Duebendorfer, E.M., and Sharp, W.D., 2001, Discussion and reply, *of* Variation in displacement along strike of the South Virgin–White Hills detachment fault—Perspective from the northern White Hills, northwestern Arizona: Geological Society of America Bulletin, v. 113, p. 532–535.

Anderson, R.E., and Laney, R.W., 1975, The influence of late Cenozoic stratigraphy on distribution of impoundment-related seismicity at Lake Mead, Nevada-Arizona: U.S. Geological Survey Journal of Research, v. 3, p. 337–343.

Beard, L.S., Anderson, R.E., Block, D.L., Bohannon, R.G., Brady, R.J., Castor, S.B., Duebendorfer, E.M., Faulds, J.E., Felger, T.J., Howard, K.A., Kuntz, M.A., and Williams, V.S., 2007, Preliminary geologic map of the Lake Mead 30′ × 60′ quadrangle, Clark County, Nevada, and Mohave County, Arizona: U.S. Geological Survey Open-File Report 2007–1010, pamphlet 109 p., 3 plates, scale 1:100,000, http://pubs.usgs.gov/of/2007/1010/.

Beard, L.S., Kennedy, Jeffrey, Truini, Margot, and Felger, Tracey, 2011, Geologic map of Detrital, Hualapai, and Sacramento Valleys and surrounding areas, northwest Arizona: U.S. Geological Survey Open-File Report 2011–1225, pamphlet 43 p., scale 1:250,000, http://pubs.usgs.gov/of/2011/1225/.

Blacet, P.M., 1975, Preliminary geologic map of the Garnet Mountain quadrangle, Mohave County, Arizona: U.S. Geological Survey Open-File Report 75–93, scale 1:48,000.

Blair, W.N., 1978, Gulf of California in Lake Mead area of Arizona and Nevada during late Miocene time: American Association of Petroleum Geologists Bulletin, v. 62, p. 1159–1170.

Blair, W.N., and Armstrong, A.K., 1979, Hualapai Limestone Member of the Muddy Creek Formation—The youngest deposit predating the Grand Canyon, southeastern Nevada and northwestern Arizona: U.S. Geological Survey Professional Paper 1111, 14 p.

Blythe, N.O., 2005, Basin analysis associated with middle-Miocene detachment faulting, eastern Lake Mead region, northwest Arizona: Flagstaff, Northern Arizona University, M.S. thesis, 225 p.

Blythe, N.O., Umhoefer, P.J., Duebendorfer, E.M., and Beard, L.S., 2010, Development of the Salt Spring basin in a reentrant in the hanging wall of the South Virgin–White Hills detachment fault, Lake Mead domain, northwest Arizona, *in* Umhoefer, P.J., Beard, L.S., and Lamb, M.A., eds., Miocene tectonics of the Lake Mead Region, central Basin and Range: Geological Society of America Special Paper 463, p. 61–86, doi:10.1130/2010.2463(04).

Bohannon, R.G., 1981, Middle and late Tertiary tectonics of a part of the Basin and Range province in the vicinity of Lake Mead, Nevada and Arizona, *in* Howard, K.A., Carr, M.D., and Miller, D.M., eds., 1981, Tectonic framework of the Mojave and Sonoran Deserts, California and Arizona—Abstracts from a conference held by the U.S. Geological Survey in Menlo Park, California, November 4–6, 1980: U.S. Geological Survey Open-File Report 81–503, p. 7–9, http://pubs.usgs.gov/of/1981/0503/report.pdf.

Bohannon, R.G., 1984, Nonmarine sedimentary rocks of Tertiary age in the Lake Mead region, southeastern Nevada and northwestern Arizona: U.S. Geological Survey Professional Paper 1259, 72 p.

Brady, R., Wernicke, B., and Fryxell, J., 2000, Kinematic evolution of a large-offset continental normal fault system, South Virgin Mountains, Nevada: Geological Society of America Bulletin, v. 112, p. 1375–1397.

Cascadden, T.E., 1991, Style of volcanism and extensional tectonics in the eastern Basin and Range Province, northern Mohave County, Arizona: Las Vegas, University of Nevada, M.S. thesis, 133 p.

Crossey, L.J., Karlstrom, K.E., Dorsey, R., Pearce, J., Wan, E., Beard, L.S., Asmeron, Y., Polyak, V., Crow, R.S., Cohen, A., Bright, J., and Pecha, M.E., 2015, Importance of groundwater in propagating downward integration of the 6–5 Ma Colorado River system—Geochemistry of springs, travertines and lacustrine carbonates of the Grand Canyon region over the past 12 Ma: Geosphere, v. 11, p. 660–682, doi:10.1130 /GES01073.1.

Dickinson, W.R., Karlstrom, K.E., Hanson, A.D., Gehrels, G.E., Pecha, Mark, Cather, S.M., and Kimbrough, D.L., 2014, Detrital-zircon U-Pb evidence precludes paleo-Colorado River sediment in the exposed Muddy Creek Formation of the Virgin River depression: Geosphere, v. 10, p. 1123–1138, doi:10.1130/GES01097.1.

Duebendorfer, E.M., 2015, Refining the early history of the Mojave-Yavapai boundary zone—Rifting versus arc accretion as mechanisms for Paleoproterozoic crustal growth in southwestern Laurentia: Journal of Geology, v. 123, p. 21–38, doi:10.1086/678950.

Duebendorfer, E.M., Chamberlain, K.R., and Jones, C.S., 2001, Paleoproterozoic tectonic history of the Cerbat Mountains, northwestern Arizona—Implications for crustal assembly in the southwestern United States: Geological Society of America Bulletin, v. 113, p. 575–590.

Duebendorfer, E.M., Faulds, J.E., and Fryxell, J.E., 2010, The South Virgin-White Hills detachment fault, southeastern Nevada and northwestern Arizona—Significance, displacement gradient, and corrugation formation, *in* Umhoefer, P.J., Beard, L.S., and Lamb, M.A., eds., Miocene tectonics of the Lake Mead region, central Basin and Range: Geological Society of America Special Paper 463, p. 275–287, doi:10.1130/2010.2463(12).

Duebendorfer, E.M., and Sharp, W.D., 1998, Variation in displacement along strike of the South Virgin–White Hills detachment fault—Perspective from the northern White Hills, northwestern Arizona: Geological Society of America Bulletin, v. 110, p. 1574–1589.

Faulds, J.E., Feuerbach, D.L., Reagan, M.K., Metcalf, R.V., Gans, P., and Walker, J.D., 1995, The Mount Perkins block, northwestern Arizona—An exposed cross section of an evolving preextensional to synextensional magmatic system: Journal of Geophysical Research, v. 100, p. 15,249–15,266.

Faulds, J.E., Howard, K.A., and Duebendorfer, E., 2008, Cenozoic evolution of the abrupt Colorado Plateau-Basin and Range boundary, northwest Arizona—A tale of three basins, immense lacustrine-evaporite deposits, and the nascent Colorado River: Geological Society of America Field Guide 11, p. 119–151, doi:10.130/2008.fld011(06).

Faulds, J.E., Olson, E.L., Harlan, S.S., and McIntosh, W.C., 2002, Miocene extension and fault-related folding in the Highland Range, southern Nevada—A three-dimensional perspective: Journal of Structural Geology, v. 24, p. 861–886.

Faulds, J.E., Price, L.M., Snee, L.W., and Gans, P.B., 2010, A chronicle of Miocene extension near the Colorado Plateau-Basin and Range boundary, southern White Hills, northwestern Arizona—Paleogeographic and tectonic implications, *in* Umhoefer, P.J., Beard, L.S., and Lamb, M.A., eds., Miocene tectonics of the Lake Mead region, central Basin and Range: Geological Society of America Special Paper 463, p. 87–120, doi:10.1130/2010.2463(06).

Faulds, J.E., Schreiber, B.C., Langenheim, V.E., Hinz, N.H., Shaw, T.H., Heizler, M.T., Perkins, M.E., El Tabkh, Mohammed, and Kunk, M.J., 2016, Paleogeographic implications of late Miocene lacustrine and nonmarine evaporate deposits in the Lake Mead region—Immediate precursors to the Colorado River: Geosphere, v. 12, p. 721–767, doi:10.1130/GES01143.1.

Felger, T.J., and Beard, L.S., 2010, Geologic map of the Lake Mead and surrounding regions, southern Nevada, southwestern Utah, and northwestern Arizona, *in* Umhoefer, P.J., Beard, L.S., and Lamb, M.A., eds., Miocene tectonics of the Lake Mead region, central Basin and Range: Geological Society of America Special Paper 463, p. 29–38, 1 plate, doi:10.1130/2010.2463(02).

Felger, T.J., Beard, L.S., Anderson, Z.W., Fleck, R.J., Wooden, J.L., and Seixas, G.B., 2014, Preliminary geologic map of Black Canyon and surrounding region, Nevada and Arizona: U.S. Geological Survey Open-File Report 2013–1267–A, pamphlet 20 p., scale 1:48,000, http://pubs.usgs.gov/of/2013/1267/a/.

Fitzgerald, P.G., Duebendorfer, E.M., Faulds, J.E., and O'Sullivan, P., 2009, The South Virgin-White Hills detachment fault of SE Nevada and NW Arizona—The application of apatite fission-track thermochronology to constraining displacement gradient accommodation along a major detachment: Tectonics, v. 28, TC2001, 31 p., doi:10.1029/2007TC002194.

Fryxell, J.E., Salton, G.G., Selvertone, J., and Wernicke, B., 1992, Gold Butte crustal section, South Virgin Mountains, Nevada: Tectonics, v. 11, p. 1099–1120, doi:10.1029/92TC00457.

Hook, S.J., Dmochowski, J.E., Howard, K.A., Rowan, L.C., Karlstrom, K.E., and Stock, J.M., 2005, Variations in weight percent silica measured from remotely acquired multispectral thermal infrared data—Examples from the Hiller Mountains, Nevada, USA and Tres Virgenes-La Reforma, Baja California Sur, Mexico: Remote Sensing of Environment, v. 95, p. 273–289.

House, P.K., Pearthree, P.A., Howard, K.A., Bell, J.W., Perkins, M.E., Faulds, J.E., and Brock, A.L., 2005, Birth of the lower Colorado River—Stratigraphic and geomorphic evidence for its inception near the conjunction of Nevada, Arizona, and California, *in* Pederson, J., and Dehler, C.M., eds., Interior Western United States: Geological Society of America Field Guide 6, p. 357–387, doi:10.1130/2005.fld006(17).

Howard, K.A., Beard, L.S., Kuntz, M.A., Kunk, M.J., Sarna-Wojcicki, A.M., Perkins, M.E., and Lucchitta, Ivo, 2010, Erosion of tilted fault blocks and deposition of coarse sediments in half-graben basins during late stages of extension—Gold Butte area, Basin and Range province, *in* Umhoefer, P.J., Beard, L.S., and Lamb, M.A., eds., Miocene tectonics of the Lake Mead region, central Basin and Range: Geological Society of America Special Paper 463, p. 147–170, doi:10.1130/2010.2463(07).

Howard, K.A., and Bohannon, R.G., 2001, Lower Colorado River—Framework, Neogene deposits, incision, and evolution, *in* Young, R.A., and Spamer, E.E., eds., The Colorado River—Origin and evolution: Grand Canyon, Ariz., Grand Canyon Association Monograph 12, p. 101–105.

Howard, K.A., Faulds, J.E., Beard, L.S., and Kunk, M.J., 2000, Reverse-drag folding across the path of the antecedent early Pliocene Colorado River below the mouth of the Grand Canyon—Implications for plateau uplift [abs.]: Geological Society of America Abstracts with Programs, v. 32, no. 7, p. A41.

Howard, K.A., Hook, S.J., Phelps, G.A., and Block, D.L., 2003, Geologic map of the Hiller Mountains quadrangle, Clark County, Nevada and Mohave County, Arizona: Nevada Bureau of Mines and Geology Map 137, scale 1:24,000, pamphlet 8 p., http://pubs.nbmg.unr.edu/Geologic-Hiller-Mts-quad-p/m137.htm.

Howard, K.A., House, P.K., Dorsey, R.J., and Pearthree, P.A., 2015, River-evolution and tectonic implications of a major Pliocene aggradation on the lower Colorado River—The Bullhead Alluvium: Geosphere, v. 11, p. 1–30, doi:10.1130/GES01059.1.

Howard, K.A., Lundstrom, S.C., Malmon, D.V., and Hook, S.J., 2008, Age, distribution, and formation of late Cenozoic paleovalleys of the lower Colorado River and their relation to river aggradation and degradation, *in* Reheis, M.C., Herschler, R., and Miller, D.M., eds., Late Cenozoic drainage history of the southwestern Great Basin and Lower Colorado River region—Geologic and biotic perspectives: Geological Society of America Special Paper 439, p. 389–408, doi:10.1130/2008.2439(18).

Kimbrough, D.L., Grove, Marty, Gehrels, G.E., Dorsey, R.J., Howard, K.A., Lovera, Oscar, Aslan, Andres, House, P.K., and Pearthree, P.A., 2015, Detrital zircon U-Pb provenance of the Colorado

River—A five million year record of incision into cover strata overlying the Colorado Plateau and adjacent regions: Geosphere, v. 11, p. 1719–1748, doi:10.1130/GES00982.

Laney, R.L., 1979a, Geohydrologic reconnaissance of Lake Mead National Recreation Area—Temple Bar to Grand Wash Cliffs, Arizona: U.S. Geological Survey Open-File Report 79–688, 72 p.

Laney, R.L., 1979b, Geohydrologic reconnaissance of Lake Mead National Recreation Area—Hoover Dam to Temple Bar, Arizona: U.S. Geological Survey Open-File Report 79–689, 42 p.

Langenheim, V.E., Beard, L.S., and Faulds, J.E., 2010, Implications of geophysical analysis on basin geometry and fault offsets in the northern Colorado River extensional corridor and adjoining Lake Mead region, Nevada and Arizona: Geological Society of America Special Paper 463, p. 39–60, doi:10.1130/2010.2463(03).

Longwell, C.R., 1936, Geology of the Boulder Reservoir floor, Arizona-Nevada: Geological Society of America Bulletin, v. 47, p. 1393–1476.

Lucchitta, Ivo, 1966, Cenozoic geology of the upper Lake Mead area adjacent to the Grand Wash Cliffs, Arizona: University Park, Pennsylvania State University, Ph.D. dissertation, 218 p.

Mariano, John, and Grauch, V.J.S., 1985, Aeromagnetic maps of the Colorado River region including the Kingman, Needles, Salton Sea, and El Centro 1° by 2° quadrangles, California, Arizona, and Nevada: U.S. Geological Survey Miscellaneous Field Studies Map MF–2023, 3 sheets, scales 1:250,000 and 1:750,000.

Mariano, John, Helferty, M.G., and Gage, T.B., 1986, Bouger and isostatic residual gravity maps of the Colorado River region, including the Kingman, Needles, Salton Sea, and El Centro quadrangles: U.S. Geological Survey Open-File Report 86–347, 7 sheets, scale 1:250,000.

Matmon, Ari, Stock, G.M., Granger, D.E., and Howard, K.A., 2012, Dating of Pliocene Colorado River sediments—Implications for cosmogenic burial dating and the evolution of the lower Colorado River: Geological Society of America Bulletin, v. 124, no. 3, p. 626–640, doi:10.1130/B30453.1

Pearce, J.C.L., Crossey, L.J., Karlstrom, K.E., Gehrels, George, Pecha, Mark, Beard, Sue, and Wan, Elmira, 2011, Syntectonic deposition and paleohydrology of the spring-fed Hualapai Limestone and implications for the 6–5 Ma integration of the Colorado River system through the Grand Canyon, *in* Beard, L.S., Karlstrom, K.E., Young, R.A., and Billingsley, G.H., CREvolution 2—Origin and evolution of the Colorado River system, workshop abstracts: U.S. Geological Survey Open-File Report 2011–1210, p. 180–185, http://pubs.usgs.gov/of/2011/1210/.

Pierce, H.W., 1973, Thick evaporates in the Basin and Range province—Arizona, *in* Coogan, A.H., ed., Fourth symposium on salt: Northern Ohio Geological Society, v. 2, p. 47–55.

Schmidt, D.L, 1994, Preliminary geologic map of the Farrier quadrangle, Clark and Lincoln Counties, Nevada: U.S. Geological Survey Open-File Report 94–625, 33 p.

Schmidt, D.L., Page, W.R., and Workman, J.B., 1996, Preliminary geologic map of the Moapa West quadrangle, Clark County, Nevada: U.S. Geological Survey Open-File Report 96–521, 18 p., scale 1:24,000.

Seixas, G.B., Reesor, P.G., Lopez-Pearce, Jessica, Karlstrom, K.E., and Crossey, L.J., 2015, Constraints on the evolution of vertical deformation and Colorado River incision near eastern lake Mead, Arizona, provided by quantitative structural mapping of the Hualapai Limestone: Geosphere, v. 11, p. 31–49, doi:10.1130/GES01096.1.

Spencer, J.E, Patchett, P.J., Pearthree, P.A., House, P.K., Sarna-Wojcicki, A.M., Wan, E., Roskowski, J.A., and Faulds, J.E., 2013, Review and analysis of the age and origin of the Pliocene Bouse Formation, lower Colorado River Valley, southwestern USA: Geosphere, v. 9, no. 3, 16 p., doi:10.1130/GES00896.1.

Spencer, J.E., Peters, Lisa, McIntosh, W.C., and Patchett, P.J., 2001, $^{40}Ar/^{39}Ar$ geochronology of the Hualapai Limestone and Bouse Formation and implications for the age of the lower Colorado River, *in*

Young, R.A., and Spamer, E.E., eds., The Colorado River—Origin and evolution: Grand Canyon, Ariz., Grand Canyon Association Monograph 12, p. 89–91.

Swadley, W.C., Schmidt, D.L., Shroba, R.R., Williams, V.S., and Hoover, D.L., 1995, Preliminary correlation of Quaternary and late Tertiary alluvial deposits in southeastern Nevada: U.S. Geological Survey Bulletin 2056–F, p. 181–202.

Swaney, Z.A., Duebendorfer, E.M., Fitzgerald, P.G., and McIntosh, W.C., 2010, New core complex model for the South Virgin-White Hills detachment and extension in the eastern Lake Mead area, southern Nevada and northwestern Arizona, *in* Umhoefer, P.J., Beard, L.S., and Lamb, M.A., eds., Miocene tectonics of the Lake Mead region, central Basin and Range: Geological Society of America Special Paper 463, p. 353–370, doi:10.1130/2010.2463(16).

Theodore, T.G., Blair, W.N., and Nash, J.T., 1987, Geology and gold mineralization of the Gold Basin-Lost Basin Mining Districts, Mohave County, Arizona: U.S. Geological Survey Professional Paper 1361, 167 p.

Umhoefer, P.J., Beard, L.S., Martin, K.L., and Blythe, Nathan, 2010a, From detachment to transtensional faulting—A model for the Lake Mead extensional domain based on new ages and correlation of subbasins, *in* Umhoefer, P.J., Beard, L.S., and Lamb, M.A., eds., Miocene tectonics of the Lake Mead region, central Basin and Range: Geological Society of America Special Paper 463, p. 371–394, doi:10.1130/2010.2463(17).

Umhoefer, P.J., Duebendorfer, E.M., Blythe, Nathan, Swaney, Z.A., Beard, L.S., and McIntosh, W.C., 2010b, Development of Gregg Basin and the southwestern Grand Wash Trough during late-stage faulting in eastern Lake Mead, Arizona, *in* Umhoefer, P.J., Beard, L.S., and Lamb, M.A., eds., Miocene tectonics of the Lake Mead region, central Basin and Range: Geological Society of America Special Paper 463, p. 221–241, doi:10.1130/2010.2463(0710).

U.S. Geological Survey, 1972, Salt anticlinal structure in Detrital Valley, Arizona, *in* U.S. Geological Survey Research 1972: U.S. Geological Survey Professional Paper 800–A, p. A43.

Verdel, Charles, Niemi, Nathan, and van der Pluijm, B.A., 2011, Thermochronology of the Salt Spring fault—Constraints on the evolution of the South Virgin-White Hills detachment system, Nevada and Arizona, USA: Geosphere, v. 7, p. 774–784, doi:10.1130/GES00616.1.

Wallace, M.W., Faulds, J.E., and Brady, R.J., 2005, Geologic map of the Meadview North quadrangle, Arizona and Nevada: Nevada Bureau of Mines and Geology Map 154, scale 1:24,000, 22 p.

Wooden, J.L., and DeWitt, Ed, 1991, Pb isotopic boundary for the boundary between the Early Proterozoic Mojave and central Arizona crustal provinces in western Arizona, *in* Karlstrom, K.E., ed., Proterozoic geology and ore deposits of Arizona: Arizona Geological Society Digest, v. 19, p. 27–50.

Young, R.A., and Hartman, J.H., 2014, Paleogene rim gravel of Arizona—Age and significance of the Music Mountain Formation: Geosphere, v. 10, p. 870–891, doi:10.1130/GES00971.1.